Postprint of: Dastjerdi, Sh.; Malikan, M.; Dimitri, R.; Tornabene, F. Nonlocal three-dimensional elasticity analysis of moderately thick porous functionally graded plates in a hygro-thermal environment. COMPOSITE STRUCTURES. (2020), 112925 DOI: 10.1016/j.compstruct.2020.112925

Nonlocal three-dimensional elasticity analysis of moderately thick porous functionally graded plates in a hygro-thermal environment

Shahriar Dastjerdi [a,b], Mohammad Malikan [c], Rossana Dimitri [d] and Francesco Tornabene [d*]

[a] Department of Mechanical Engineering, Faculty of Engineering, Islamic Azad University, Shahrood Branch, Shahrood, Iran
[b] Division of Mechanics, Civil Engineering Department, Akdeniz University, Antalya, Turkey
[c] Department of Mechanics of Materials and Structures, Faculty of Civil and Environmental Engineering, Gdańsk University of Technology, Gdańsk, Poland
[d] Department of Innovation Engineering, Università del Salento, Lecce, Italy
* **Correspondence:** author: francesco.tornabene@unisalento.it

Abstract: This work performs a novel quasi three-dimensional (3D) bending analysis for a moderately thick functionally graded material (FGM) made of nanoceramics and metal powders, in presence of porosities due to some incorrect manufacturing processes. Such porosities can appear within the plate in two forms, namely, even and uneven distributions. The modeled system assumes a polymer matrix where both shear and transverse factors coexist. The bending equations are obtained by using the Hamiltonian principle. In order to apply the quantum effects for the nanosystem, the well-known nonlocal theory of Eringen is simply assumed, while checking for its numerical accuracy. A physically-consistent analysis of the nanostructures would investigate possible surrounding effects. Thus, the thermal and humidity influence is accounted for the 3D problem, whose governing equations are solved through a semi-analytical polynomial method (SAPM), as recently proposed in literature for different applications. The proposed method is based on a simple procedure with very accurate numerical outcomes, whose performance is checked against the available literature. After computing the deflection relations, a systematic study is performed for the bending response of nanoporous FGMs in a hygro-thermal surrounding environment, with promising results for practical applications.

Keywords: Hygro-thermal-elastic problem; Moderately thick FGM; Nonlocal theory of Eringen; Porosity; Semi-analytical polynomial method

Symbols

$U(x,y,z)$: Displacement function of the plate along x direction

$V(x,y,z)$: Displacement function of the plate along y direction

$W(x,y,z)$: Displacement function of the plate along z direction

$u(x,y,z)$: Nodal kinematic displacement of the plate along the x axis

$v(x,y,z)$: Nodal kinematic displacement of the plate along the y axis

$w(x,y,z)$: Nodal kinematic displacement of the plate along the z axis

$\delta\Pi$ denote the variational form of the strain energy

z: A coordinate for the thickness changes

α Thermal expansion coefficient

ΔT : Variation of temperature concentration

ΔH : Variation of moisture concentration

$\delta\Omega$: Variational form of the external work

L_x, L_y : Length and width of the plate

k_p : In-plane effects of the polymer foundation

e_0: Depends on the type of material

δT : Variational form of the kinetic energy

$\sigma_{ij}\ (i, j = x, y, z)$: Tensor of mechanical stresses

E_m : Young's modulus for the metal phase

E_c : Young's modulus for the ceramic phase

k_w : Transverse effect of the polymer foundation

β : Hygral expansion coefficient

L: Local analysis

NL: Nonlocal analysis

μ: Nonlocal parameter

ε_{xx} : Axial strain along x axis

ε_{yy} : Axial strain along y axis

ε_{zz} : Transverse strain along z axis

γ_{xy} : Shear strain in x-y plan

γ_{yz} : Shear strain in y-z plan

γ_{xz} : Shear strain in x-z plan

a : A length scale

h: Plate's thickness

g: Grading index

q_z: Transverse loading

t : Time variable

1. Introduction

In the last decades the increased adoption of functionally graded materials (FGMs), has been mainly related to the gradual reduction of the internal thermal stresses of materials at high temperatures. Differently from classical composite materials with distinct substrates and sudden variations of properties, a functional variation of material properties is ensured in FGMs, such as thermal resistance, thermal conductivity and coefficient of thermal expansion. An abrupt change in the coefficient of thermal expansion throughout a joint (interface of two layers) leads to a meaningful internal thermal stress at high temperatures that could lead to the interfacial collapse [1]. In 1988, the basic concept of FGMs was developed to reduce thermal stresses within materials, and the well-known FGMs association was established in Japan [2], focusing on layered materials (i.e. structural materials, biomaterials, semiconductor and conductive materials) with continuously and gradually changing properties [2].

In a context where the scientific community reveals an increased attention to nanoscience and nanotechnology as new form of manufacturing materials, while controlling and manipulating their structural units at nanoscale levels, FGMs have been successfully applied for many practical applications [3]. In fact, a functional nanoscale material includes the beneficial properties of nanostructures and functional grading materials. Among the recent studies from the literature on the mechanical response of FGMs, Dastjerdi and Akgöz [4] analyzed the statics and dynamics a macro/nano functional grading thick plates embedded in a thermal surround based on an exact three-dimensional theory of elasticity. The nonlocal theory of elasticity was employed to capture nanoscale effects, whereby a SAPM was applied to compute the structural deflection. Based on the application of a three-dimensional approach, the thermal environment was found to yield a structural deflection even after the removal of the external mechanical load. On the other hand,

plate theories that do not account for the transverse static load, the thermal environment does not affect the mechanical response, such that deflections maintain equal to zero. An interesting analytical study of the stability response for nanoporous FGMs with even and uneven porosity distributions, was proposed by Malikan et al. [5] based on the nonlocal theory of Eringen, whose solutions were found by means of the volume integrals. In a further work by Ansari et al. [6], the three-dimensional elasticity was combined to the nonlocal continuum approach to check for the natural frequencies of graded nanosheets embedded in a polymer foundation, and solved the problem numerically through the generalized differential quadrature method. Moreover, Malikan et al. [7] proposed a modified version of the Timoshenko beam theory to examine the transient behavior of viscoelastic nanotubes, which was verified in its efficiency by means of a comparative evaluation with the available literature. Brischetto [8] derived a novel three-dimensional formulation for the study of the static behavior of single and multi-layer plates and shells. The problem was solved numerically for simply-supported structures by means of the exponential matrix method. Similar problems were explored by Ansari et al. [9] for functionally graded (FG) nonlocal plates under a static and dynamic loading, while applying successfully the differential quadrature technique, whose efficiency has been largely verified in many recent works, see [10-13], among others.

Dastjerdi et al. [14] presented a novel approach for the static study of double-layered conical nanopanels including the presence of the van der Waals interactions, modeled as nonlinear springs. In some further works, the same authors applied the first-order shear deformation theory [15,16] or a higher-order shear deformation theory [17] to analyze the structural local and nonlocal behavior of annular sector sheets. In line with the previous works, Salehipour et al. [18] solved the static problem of FG micro and nanosheets, where a polymer substrate was fixed under the plate and a modified couple stress method was employed to account for the length scale effects on the structural behavior.

In the context of coupled thermo-mechanical problems many works have been treated numerically or computationally by the scientific community for nanostructures with different geometries. Alibeigloo [19] analyzed numerically the thermoelastic response of a sandwich plate made of a FG core, and subjected to a thermal shock, based on the Fourier series expansions.

Possible effects of porosities on the thermomechanical response of plates can be found in [20], where the structure was immersed in a thermal surround, whereby in another work, Dastjerdi et al. [21] showed the influences of vacancy in graphene nanoplates subjected uniformly to a transverse static load. Other coupled thermo-mechanical studies of multilayered sheets and structures with different geometries can be found in [22-24], whereby Wang [25] accounted for the possible exposure of porous FG structures to an electrical field, and its effect on their frequency response.

In this last work, the nonlocal elasticity approach was combined with the first-order shear deformation theory, and the differential quadrature technique was applied to solve the equations of the problem. In addition, Jouneghani et al. [26] analyzed the thermo-hygro elastic behavior of a nonlocal FG beam subjected to in-plane forces. Malikan et al. [27] focused on the vibration of nanotubes in an external damping condition and a thermal environment. The thermo-vibrational equations of the problem were derived based on a novel beam theory in conjunction with a higher-order nonlocal strain gradient theory. Fares et al. [28] investigated the free vibration and bending response of a FG shell with a doubly-curved geometry modeled through a multiple stratification. An enhanced layerwise theory was also used to drive the energy formulation. A different numerical tool based on a meshless method was applied by Sator et al. [29] for the thermoelastic study of FGM plates under a static loading condition. Higher-order nonlocal strain gradient theories involving different length scales were applied in [30, 31] for the study of the excited frequencies and critical stability loads under coupled electro-magnetic conditions. The first example of a viscoelastic nanoplate with a corrugated geometry was explored by Malikan et al. [32], where a vibrational problem was tackled trough a nonlocal strain gradient model and solved analytically according to

the Navier technique. Additional works on the topic can be found in [33-40] for different structural analyses of nanostructures and external conditions.

As far as the three-dimensional elasticity analysis of nanostructures is concerned, different semi-analytical approaches, mixed formulations, and/or numerical methods have been adopted in literature to tackle the problem, see refs. [41-45], among others. More specifically, Lomte Patil et al. [42] solved three-dimensional elasticity relations by comparing several advanced approaches available from the literature. Dastjerdi and Jabbarzadeh [43] applied the nonlocal theory of Eringen for the structural study in static conditions of a double-layered rectangular graphene nanoplate in a continuum schema. The differential quadrature method and the SAPM were validated by the authors against the literature for several boundary conditions of the nanostructures. In the additional works by Dastjerdi et al. [44-46], different single-layer [44], bilayer [45] and multi-layer [46] annular/circular nanosheets on an elastic foundation were explored under a static transverse uniform loading, while employing the first-order shear deformation theory in conjunction with the nonlocal theory of Eringen. Possible effects on the mechanical behavior of nanostructures has been also studied in [47-52], always by involving combined versions of the nonlocal strain gradient model. More in detail, in Ref. [47] the dynamic stability of graphene sheets located on a visco-elastic medium was studied by using the neperian frequencies, while in [48] the three-dimensional elasticity problem was approached by means of the nonlocal theory of strain gradient theory in order to study an anisotropic FG spherical sample. She et al. [49] determined the natural frequencies and nonlinear static deflections of FG nanobeams by means of a nonlocal theory of strain gradient formulation. Ahmed Hasan and Kurgan [50] predicted critical buckling loads for FGM plate in the skew form while the plate was embedded in the Winkler matrix. A new study on the fullerene was done by Dastjerdi and Akgöz [51], in which a static bending analysis was conducted by a nonlocal model and solved with respect to the SAPM method.

To a large extent, a smart nanomachine's application depend on its nano parts, e.g. multifunctional sensors, actuators and etc. Piezoelectric sensors of nanomachines require large deformations to generate an appreciable electric voltage [53]. Electric voltage can be produced by strains as a result of transverse deflection. However, negligible electricity will be created by simple bending of a nano sensor. In light of the fact that poling direction in electromechanical sensors is same with the thickness direction according to the transverse electric field, any extra deformation plays vital role in generating electricity. The case is simple, let us divide the thickness into two sections, upper than mid-plan and lower than it. Hence, polarization in the upper section of thickness due to tension will cancel the polarization in the lower section due to compression. Therefore, thickness's changes of the nano piezoelectric sensor lead to unsymmetrical deformation in the sensor and then can make it more efficient due to more capability of sensor to emergence stronger electric field. So, understanding both transverse deflection of a nano part beside its thickness variations will let us to design more precise these momentous smart parts. Although, this research does not consider a piezoelectric nano part, the effect of deformation in thickness of a functional nano part would be exhibited whilst deflections in all surfaces of thickness can be observed.

Based on the above-mentioned literature, however, there is a general lack of attention to the possible effect of porosity on the three-dimensional elasticity analysis of composite nanoplates. This aspect is herein explored, while proposing a novel three-dimensional elasticity analysis and a nonlocal continuum theory, accounting for small scale effects. To this end, a moderately thick nanoplate FGM with porosity is considered, immersed in a hygro-thermal environment, including possible further effects related to the moisture and temperature parameters. The system is bridged on a two-parameter polymeric medium. To solve the problem, the SAPM is successfully employed as already proposed by the same authors in the previous literature for different applications. A large parametric study investigates the sensitivity of the three-dimensional bending response of porous nanoplates for several interior factors, i.e. nonlocality, length scale parameter, porosity, and hygrothermal impact. The work is organized as follows. Section 2 describes the mathematical

problem, for which a SAP solution is proposed in Section 3. Section 4 illustrates the numerical results from a large parametric investigation, and some remarkable conclusions are discussed finally in Section 5.

2. Mathematical modelling

Let us consider a nano porous FG rectangular sheet (see Figure 1) with in-plane dimensions L_x , L_y along the x , y directions, respectively, and thickness h . Three-dimensional partial differential elastic equations of a similar problem, are challenging and costly to be solved, such that bi-dimensional theories are usually preferred by engineers and mathematicians in literature.

By considering the strain variation along the thickness leads to more accurate results, especially for moderately thick sheets, where numerical errors could be reduced especially in presence of coupled problems. In this context, the key point of the present research is to examine through-the-thickness strain variation, by proposing an accurate three-dimensional approach, while limiting the numerical cost. Based on the three-dimensional elasticity approach, the displacement field is assumed as [4-5]

$$\begin{aligned} U(x,y,z,t) &= u(x,y,z) \\ V(x,y,z,t) &= v(x,y,z) \\ W(x,y,z,t) &= w(x,y,z) \end{aligned} \tag{1a-c}$$

in which $U(x,y,z)$, $V(x,y,z)$ and $W(x,y,z)$ are the displacement functions of the plate along x, y and z directions, and $u(x,y,z)$, $v(x,y,z)$ and $w(x,y,z)$ refer to the nodal kinematic displacement of the plate along the mentioned axes. These kinematic variables depend on the grid points locations, with the distribution represented in Figure 2. Furthermore, t exhibits the time variable in a dynamic analysis. Applying strains of Lagrangian on Equations (1) and based on the variational energy and minimizing the total potential energy of the system, the actual three-dimensional displacement field yields to the following governing equations (see Ref. [5]), for which a very hard solving process would be required. It should be noted that the nonlinear terms (e.g. $\frac{\partial \sigma_{xz}}{\partial z}\frac{\partial w}{\partial x}$ in Eq. (2c)) are considered in obtained governing equations. Nonlinear analysis gives more accurate results specially for large deformations. However, the number of calculations increases dramatically which is challenging in solution process. Neglecting nonlinear terms (in Eq. (2c)) can be possible for small and moderate deformations such as buckling analysis.

$$\frac{\partial \sigma_x}{\partial x}+\frac{\partial \sigma_{xy}}{\partial y}+\frac{\partial \sigma_{xz}}{\partial z}=0 \tag{2a}$$

$$\frac{\partial \sigma_{xy}}{\partial x}+\frac{\partial \sigma_y}{\partial y}+\frac{\partial \sigma_{yz}}{\partial z}=0 \tag{2b}$$

$$\begin{aligned} &\frac{\partial \sigma_{xz}}{\partial x}\left(1+\frac{\partial w}{\partial z}\right)+\frac{\partial \sigma_{xz}}{\partial z}\frac{\partial w}{\partial x}+\frac{\partial \sigma_{yz}}{\partial y}\left(1+\frac{\partial w}{\partial z}\right)+\frac{\partial \sigma_{yz}}{\partial z}\frac{\partial w}{\partial y}+2\sigma_{xz}\frac{\partial^2 w}{\partial x\,\partial z} \\ &+2\sigma_{yz}\frac{\partial^2 w}{\partial y\,\partial z}+\sigma_x\frac{\partial^2 w}{\partial x^2}+\sigma_y\frac{\partial^2 w}{\partial y^2}+2\sigma_{xy}\frac{\partial^2 w}{\partial x\,\partial y}+\sigma_z\frac{\partial^2 w}{\partial z^2}+\frac{\partial \sigma_z}{\partial z}\left(1+\frac{\partial w}{\partial z}\right)=0 \end{aligned} \tag{2c}$$

in which $\sigma_{ij}\,(i,j=x,y,z)$ represents the tensor of mechanical stresses. However, according to a quasi-three-dimensional elasticity field, as proposed in this work, the solution procedure would be much easier, since grid points distribution refers to a bi-dimensional domain. Thus, the equilibrium relations would be derived starting with the following definition of the kinematic field

$$U(x,y,z)=u_1(x,y)+zu_2(x,y)+z^2u_3(x,y)+z^3u_4(x,y)+z^4u_5(x,y)+z^5u_6(x,y)$$
$$V(x,y,z)=v_1(x,y)+zv_2(x,y)+z^2v_3(x,y)+z^3v_4(x,y)+z^4v_5(x,y)+z^5v_6(x,y) \quad (3a\text{-}c)$$
$$W(x,y,z)=w_1(x,y)+zw_2(x,y)+z^2w_3(x,y)+z^3w_4(x,y)+z^4w_5(x,y)+z^5w_6(x,y)$$

in which z symbolizes a coordinate for the thickness changes. Also, the strain field can be formulated as follows

$$\varepsilon_{xx}=\frac{\partial U}{\partial x};\varepsilon_{yy}=\frac{\partial V}{\partial y};\varepsilon_{zz}=\frac{\partial W}{\partial z}$$
$$\gamma_{xz}=\frac{1}{2}\left(\frac{\partial U}{\partial z}+\frac{\partial W}{\partial x}\right);\gamma_{xy}=\frac{1}{2}\left(\frac{\partial U}{\partial y}+\frac{\partial V}{\partial x}\right);\gamma_{yz}=\frac{1}{2}\left(\frac{\partial V}{\partial z}+\frac{\partial W}{\partial y}\right) \quad (4a\text{-}f)$$

By combination of Equations (3) and (4) we get

$$\varepsilon_{xx}=\frac{\partial u_1}{\partial x}+z\frac{\partial u_2}{\partial x}+z^2\frac{\partial u_3}{\partial x}+z^3\frac{\partial u_4}{\partial x}+z^4\frac{\partial u_5}{\partial x}+z^5\frac{\partial u_6}{\partial x} \quad (5a)$$
$$\varepsilon_{yy}=\frac{\partial v_1}{\partial y}+z\frac{\partial v_2}{\partial y}+z^2\frac{\partial v_3}{\partial y}+z^3\frac{\partial v_4}{\partial y}+z^4\frac{\partial v_5}{\partial y}+z^5\frac{\partial v_6}{\partial y} \quad (5b)$$
$$\varepsilon_{zz}=w_2+2zw_3+3z^2w_4+4z^3w_5+5z^4w_6 \quad (5c)$$
$$\gamma_{xy}=\frac{\partial v_1}{\partial x}+z\frac{\partial v_2}{\partial x}+z^2\frac{\partial v_3}{\partial x}+z^3\frac{\partial v_4}{\partial x}+z^4\frac{\partial v_5}{\partial x}+z^5\frac{\partial v_6}{\partial x}$$
$$+\frac{\partial u_1}{\partial y}+z\frac{\partial u_2}{\partial y}+z^2\frac{\partial u_3}{\partial y}+z^3\frac{\partial u_4}{\partial y}+z^4\frac{\partial u_5}{\partial y}+z^5\frac{\partial u_6}{\partial y} \quad (5d)$$
$$\gamma_{xz}=\frac{\partial w_1}{\partial x}+z\frac{\partial w_2}{\partial x}+z^2\frac{\partial w_3}{\partial x}+z^3\frac{\partial w_4}{\partial x}+z^4\frac{\partial w_5}{\partial x}$$
$$+z^5\frac{\partial w_6}{\partial x}+u_2+2zu_3+3z^2u_4+4z^3u_5+5z^4u_6 \quad (5e)$$
$$\gamma_{yz}=\frac{\partial w_1}{\partial y}+z\frac{\partial w_2}{\partial y}+z^2\frac{\partial w_3}{\partial y}+z^3\frac{\partial w_4}{\partial y}+z^4\frac{\partial w_5}{\partial y}$$
$$+z^5\frac{\partial w_6}{\partial y}+v_2+2zv_3+3z^2v_4+4z^3v_5+5z^4v_6 \quad (5f)$$

As far as the hygro-thermal surround is concerned, the mechanical strain field should be combined with thermal and hygral ones as follows [31],

$$\sigma_{ij}=C_{ijkl}:\left[\varepsilon_{kl}^{mech}-\varepsilon_{kl}^{Thermal}-\varepsilon_{kl}^{Hygral}\right] \quad (6)$$

and

$$\varepsilon^{Thermal}=\alpha\Delta T \quad (7a)$$
$$\varepsilon^{Hygral}=\beta\Delta H \quad (7b)$$

α and β being the thermal and hygral expansion coefficients. In addition, ΔT and ΔH in Equations (7) refer to the variation of temperature and moisture concentration, respectively [31].

In this paper, a FG nanoplate is assumed, whose thermoelastic material properties vary as [4-5]

$$E(z)=E_m+(E_c-E_m)\left(\frac{1}{2}+\frac{z}{h}\right)^g \quad (8a)$$

$$\alpha(z)=\alpha_m+(\alpha_c-\alpha_m)\left(\frac{1}{2}+\frac{z}{h}\right)^g \tag{8b}$$

where E_m and E_c stand for the Young's modulus for the metal and ceramic phase, h is the plate's thickness. The Poisson's ratio is assumed that to be constant along the z direction, because of its meaningless variation in that direction. The index g in the Equation (8) refers to the material grading index, which assumed a null value, i.e. $g=0$, for a pure ceramic, whereas $g\to\infty$, for a pure metal.

Porosity yields a different response for the model proposed in [5], such that it is highly recommended to take into account such manufacturing defect, for an appropriate estimation of the mechanical behavior especially in presence of FG material properties. Thus, the Young's modulus for FG plates with even or uneven porosities takes the following form [5]

$$E(z)=E_m+(E_c-E_m)\left(\frac{1}{2}+\frac{z}{h}\right)^g-\frac{\lambda}{2}(E_c+E_m) \tag{9a}$$

$$E(z)=E_m+(E_c-E_m)\left(\frac{1}{2}+\frac{z}{h}\right)^g-\frac{\lambda}{2}(E_c+E_m)\left(1-\frac{2|z|}{h}\right) \tag{9b}$$

in which λ denotes the type of porosities distribution.

In this paper, the governing equations and boundary conditions of the problem have been derived based on the principle of minimum potential energy. According to the Hamiltonian law, the variation of the potential energy F must be zero, namely

$$\delta F=\delta\int_0^t(\Pi+\Omega-T)dt=0 \tag{10}$$

where $\delta\Omega$, δT and $\delta\Pi$ denote the variational form of the external work, the kinetic energy (equal to zero because of the static analysis here is considered), and the strain energy. The bending problem is defined as reported in what follows.

First, we define the strain energy in a virtual form as

$$\delta\Pi=\iiint_v\left(\sigma_{xx}\delta\varepsilon_{xx}+\sigma_{yy}\delta\varepsilon_{yy}+\sigma_{zz}\delta\varepsilon_{zz}+\sigma_{xy}\delta\varepsilon_{xy}+\sigma_{xz}\delta\varepsilon_{xz}+\sigma_{yz}\delta\varepsilon_{yz}\right)dxdydz=0 \tag{11}$$

By using Equations (5) and (11), the energy formulation can be written as below

$$\begin{aligned}\delta\Pi=\iiint_V\Bigg(&\sigma_{xx}\left[\frac{\partial\delta u_1}{\partial x}+z\frac{\partial\delta u_2}{\partial x}+z^2\frac{\partial\delta u_3}{\partial x}+z^3\frac{\partial\delta u_4}{\partial x}+z^4\frac{\partial\delta u_5}{\partial x}+z^5\frac{\partial\delta u_6}{\partial x}\right]\\&+\sigma_{yy}\left[\frac{\partial\delta v_1}{\partial y}+z\frac{\partial\delta v_2}{\partial y}+z^2\frac{\partial\delta v_3}{\partial y}+z^3\frac{\partial\delta v_4}{\partial y}+z^4\frac{\partial\delta v_5}{\partial y}+z^5\frac{\partial\delta v_6}{\partial y}\right]\\&+\sigma_{zz}\left[\delta w_2+2z\delta w_3+3z^2\delta w_4+4z^3\delta w_5+5z^4\delta w_6\right]\\&+\sigma_{xy}\left[\frac{\partial\delta v_1}{\partial x}+z\frac{\partial\delta v_2}{\partial x}+z^2\frac{\partial\delta v_3}{\partial x}+z^3\frac{\partial\delta v_4}{\partial x}+z^4\frac{\partial\delta v_5}{\partial x}+z^5\frac{\partial\delta v_6}{\partial x}+\frac{\partial\delta u_1}{\partial y}+z\frac{\partial\delta u_2}{\partial y}\right.\end{aligned}$$

$$+z^2\frac{\partial\delta u_3}{\partial y}+z^3\frac{\partial\delta u_4}{\partial y}+z^4\frac{\partial\delta u_5}{\partial y}+z^5\frac{\partial\delta u_6}{\partial y}\Big]+\sigma_{xz}\Big[\frac{\partial\delta w_1}{\partial x}+z\frac{\partial\delta w_2}{\partial x}+z^2\frac{\partial\delta w_3}{\partial x}$$
$$+z^3\frac{\partial\delta w_4}{\partial x}+z^4\frac{\partial\delta w_5}{\partial x}+z^5\frac{\partial\delta w_6}{\partial x}+\delta u_2+2z\delta u_3+3z^2\delta u_4+4z^3\delta u_5+5z^4\delta u_6\Big]+$$
$$\sigma_{yz}\Big[\frac{\partial\delta w_1}{\partial y}+z\frac{\partial\delta w_2}{\partial y}+z^2\frac{\partial\delta w_3}{\partial y}+z^3\frac{\partial\delta w_4}{\partial y}+z^4\frac{\partial\delta w_5}{\partial y}+z^5\frac{\partial\delta w_6}{\partial y}$$
$$+\delta v_2+2z\delta v_3+3z^2\delta v_4+4z^3\delta v_5+5z^4\delta v_6\Big]\Big)dxdydz=0 \tag{12}$$

where the stress resultants can be defined as

$$\left\{N_{xx},N_{yy},N_{zz},N_{xy},N_{xz},N_{yz}\right\}=\int_{-\frac{h}{2}}^{+\frac{h}{2}}\left\{\sigma_{xx},\sigma_{yy},\sigma_{zz},\sigma_{xy},\sigma_{xz},\sigma_{yz}\right\}dz \tag{13a}$$

$$\left\{M_{xx},M_{yy},M_{zz},M_{xy},M_{xz},M_{yz}\right\}=\int_{-\frac{h}{2}}^{+\frac{h}{2}}\left\{\sigma_{xx},\sigma_{yy},\sigma_{zz},\sigma_{xy},\sigma_{xz},\sigma_{yz}\right\}zdz \tag{13b}$$

$$\left\{P_{xx},P_{yy},P_{zz},P_{xy},P_{xz},P_{yz}\right\}=\int_{-\frac{h}{2}}^{+\frac{h}{2}}\left\{\sigma_{xx},\sigma_{yy},\sigma_{zz},\sigma_{xy},\sigma_{xz},\sigma_{yz}\right\}z^2dz \tag{13c}$$

$$\left\{H_{xx},H_{yy},H_{zz},H_{xy},H_{xz},H_{yz}\right\}=\int_{-\frac{h}{2}}^{+\frac{h}{2}}\left\{\sigma_{xx},\sigma_{yy},\sigma_{zz},\sigma_{xy},\sigma_{xz},\sigma_{yz}\right\}z^3dz \tag{13d}$$

$$\left\{Y_{xx},Y_{yy},Y_{zz},Y_{xy},Y_{xz},Y_{yz}\right\}=\int_{-\frac{h}{2}}^{+\frac{h}{2}}\left\{\sigma_{xx},\sigma_{yy},\sigma_{zz},\sigma_{xy},\sigma_{xz},\sigma_{yz}\right\}z^4dz \tag{13e}$$

$$\left\{S_{xx},S_{yy},S_{zz},S_{xy},S_{xz},S_{yz}\right\}=\int_{-\frac{h}{2}}^{+\frac{h}{2}}\left\{\sigma_{xx},\sigma_{yy},\sigma_{zz},\sigma_{xy},\sigma_{xz},\sigma_{yz}\right\}z^5dz \tag{13f}$$

Thus, Equation (12) can be formulated by considering the stress resultants as follows

$$\delta\Pi=\iint_A\Big(\Big[N_{xx}\frac{\partial\delta u_1}{\partial x}+M_{xx}\frac{\partial\delta u_2}{\partial x}+P_{xx}\frac{\partial\delta u_3}{\partial x}+H_{xx}\frac{\partial\delta u_4}{\partial x}+Y_{xx}\frac{\partial\delta u_5}{\partial x}+S_{xx}\frac{\partial\delta u_6}{\partial x}\Big]$$
$$+\Big[N_{yy}\frac{\partial\delta v_1}{\partial y}+M_{yy}\frac{\partial\delta v_2}{\partial y}+P_{yy}\frac{\partial\delta v_3}{\partial y}+H_{yy}\frac{\partial\delta v_4}{\partial y}+Y_{yy}\frac{\partial\delta v_5}{\partial y}+S_{yy}\frac{\partial\delta v_6}{\partial y}\Big]$$
$$+\Big[N_{zz}\delta w_2+2M_{zz}\delta w_3+3P_{zz}\delta w_4+4H_{zz}\delta w_5+5Y_{zz}\delta w_6\Big]$$
$$+\Big[N_{xy}\frac{\partial\delta v_1}{\partial x}+M_{xy}\frac{\partial\delta v_2}{\partial x}+P_{xy}\frac{\partial\delta v_3}{\partial x}+H_{xy}\frac{\partial\delta v_4}{\partial x}+Y_{xy}\frac{\partial\delta v_5}{\partial x}+S_{xy}\frac{\partial\delta v_6}{\partial x}+$$
$$N_{xy}\frac{\partial\delta u_1}{\partial y}+M_{xy}\frac{\partial\delta u_2}{\partial y}+P_{xy}\frac{\partial\delta u_3}{\partial y}+H_{xy}\frac{\partial\delta u_4}{\partial y}+Y_{xy}\frac{\partial\delta u_5}{\partial y}+S_{xy}\frac{\partial\delta u_6}{\partial y}\Big]+$$
$$\Big[N_{xz}\frac{\partial\delta w_1}{\partial x}+M_{xz}\frac{\partial\delta w_2}{\partial x}+P_{xz}\frac{\partial\delta w_3}{\partial x}+H_{xz}\frac{\partial\delta w_4}{\partial x}+Y_{xz}\frac{\partial\delta w_5}{\partial x}+S_{xz}\frac{\partial\delta w_6}{\partial x}$$
$$+N_{xz}\delta u_2+2M_{xz}\delta u_3+3P_{xz}\delta u_4+4H_{xz}\delta u_5+5Y_{xz}\delta u_6\Big]+$$
$$\Big[N_{yz}\frac{\partial\delta w_1}{\partial y}+M_{yz}\frac{\partial\delta w_2}{\partial y}+P_{yz}\frac{\partial\delta w_3}{\partial y}+H_{yz}\frac{\partial\delta w_4}{\partial y}+Y_{yz}\frac{\partial\delta w_5}{\partial y}+S_{yz}\frac{\partial\delta w_6}{\partial y}$$
$$+N_{yz}\delta v_2+2M_{yz}\delta v_3+3P_{yz}\delta v_4+4H_{yz}\delta v_5+5Y_{yz}\delta v_6\Big]\Big)dxdy=0 \tag{14}$$

The external work related to the transverse loading q_z acting on the structure is expressed as [43]

$$\delta\Omega = \iint_A \left(q_z - k_w W\left(x,y,z\right) + k_p \nabla^2 W\left(x,y,z\right)\right)\delta W\left(x,y,z\right)dxdy = 0 \tag{15}$$

where k_w and k_p refer to the transverse and in-plane effects of the polymer foundation. After a mathematical manipulation, Equation (15) can be expanded as

$$\begin{aligned}
\delta\Omega = \iint_A \Big[& q_z - k_w \left(w_1 + z w_2 + z^2 w_3 + z^3 w_4 + z^4 w_5 + z^5 w_6\right) + \\
& k_p \nabla^2 \left(w_1 + z w_2 + z^2 w_3 + z^3 w_4 + z^4 w_5 + z^5 w_6\right)\Big] \\
& \left(\delta w_1 + z\,\delta w_2 + z^2 \delta w_3 + z^3 \delta w_4 + z^4 \delta w_5 + z^5 \delta w_6\right) dxdy = 0 \\
\nabla^2 = & \left(\frac{\partial^2}{\partial x^2} + \frac{\partial^2}{\partial y^2} + \frac{\partial^2}{\partial z^2}\right)
\end{aligned} \tag{16}$$

Substituting Equation (14) and (16) into Equation (10) and after integration by parts, the local governing equations can be obtained as

$$\delta u_1 : \frac{\partial N_{xx}}{\partial x} + \frac{\partial N_{xy}}{\partial y} = 0 \tag{17a}$$

$$\delta u_2 : \frac{\partial M_{xx}}{\partial x} + \frac{\partial M_{xy}}{\partial y} - N_{xz} = 0 \tag{17b}$$

$$\delta u_3 : \frac{\partial P_{xx}}{\partial x} + \frac{\partial P_{xy}}{\partial y} - 2M_{xz} = 0 \tag{17c}$$

$$\delta u_4 : \frac{\partial H_{xx}}{\partial x} + \frac{\partial H_{xy}}{\partial y} - 3P_{xz} = 0 \tag{17d}$$

$$\delta u_5 : \frac{\partial Y_{xx}}{\partial x} + \frac{\partial Y_{xy}}{\partial y} - 4H_{xz} = 0 \tag{17e}$$

$$\delta u_6 : \frac{\partial S_{xx}}{\partial x} + \frac{\partial S_{xy}}{\partial y} - 5Y_{xz} = 0 \tag{17f}$$

$$\delta v_1 : \frac{\partial N_{yy}}{\partial y} + \frac{\partial N_{xy}}{\partial x} = 0 \tag{18a}$$

$$\delta v_2 : \frac{\partial M_{yy}}{\partial y} + \frac{\partial M_{xy}}{\partial x} - N_{yz} = 0 \tag{18b}$$

$$\delta v_3 : \frac{\partial P_{yy}}{\partial y} + \frac{\partial P_{xy}}{\partial x} - 2M_{yz} = 0 \tag{18c}$$

$$\delta v_4 : \frac{\partial H_{yy}}{\partial y} + \frac{\partial H_{xy}}{\partial x} - 3P_{yz} = 0 \tag{18d}$$

$$\delta v_5 : \frac{\partial Y_{yy}}{\partial y} + \frac{\partial Y_{xy}}{\partial x} - 4H_{yz} = 0 \tag{18e}$$

$$\delta v_6 : \frac{\partial S_{yy}}{\partial y} + \frac{\partial S_{xy}}{\partial x} - 5Y_{yz} = 0 \tag{18f}$$

$$\delta w_1 : \frac{\partial N_{xz}}{\partial x}+\frac{\partial N_{yz}}{\partial y}+q_z-k_w\left(w_1+w_2\left(\frac{h}{2}\right)+w_3\left(\frac{h}{2}\right)^2+w_4\left(\frac{h}{2}\right)^3+w_5\left(\frac{h}{2}\right)^4\right.$$
$$\left.+w_6\left(\frac{h}{2}\right)^5\right)+k_p\left(\nabla^2 w_1+\nabla^2 w_2\left(\frac{h}{2}\right)+\nabla^2 w_3\left(\frac{h}{2}\right)^2+\nabla^2 w_4\left(\frac{h}{2}\right)^3+\nabla^2 w_5\left(\frac{h}{2}\right)^4\right. \quad (19a)$$
$$\left.+\nabla^2 w_6\left(\frac{h}{2}\right)^5\right)=0$$

$$\delta w_2 : \frac{\partial M_{xz}}{\partial x}+\frac{\partial M_{yz}}{\partial y}-N_{zz}+q_z\left(\frac{h}{2}\right)-k_w\left(w_1\left(\frac{h}{2}\right)+w_2\left(\frac{h}{2}\right)^2+w_3\left(\frac{h}{2}\right)^3+w_4\left(\frac{h}{2}\right)^4\right.$$
$$\left.+w_5\left(\frac{h}{2}\right)^5+w_6\left(\frac{h}{2}\right)^6\right)+k_p\left(\nabla^2 w_1\left(\frac{h}{2}\right)+\nabla^2 w_2\left(\frac{h}{2}\right)^2+\nabla^2 w_3\left(\frac{h}{2}\right)^3+\nabla^2 w_4\left(\frac{h}{2}\right)^4\right. \quad (19b)$$
$$\left.+\nabla^2 w_5\left(\frac{h}{2}\right)^5+\nabla^2 w_6\left(\frac{h}{2}\right)^6\right)=0$$

$$\delta w_3 : \frac{\partial P_{xz}}{\partial x}+\frac{\partial P_{yz}}{\partial y}-2M_{zz}+q_z\left(\frac{h}{2}\right)^2-k_w\left(w_1\left(\frac{h}{2}\right)^2+w_2\left(\frac{h}{2}\right)^3+w_3\left(\frac{h}{2}\right)^4+\right.$$
$$\left.w_4\left(\frac{h}{2}\right)^5+w_5\left(\frac{h}{2}\right)^6+w_6\left(\frac{h}{2}\right)^7\right)+k_p\left(\nabla^2 w_1\left(\frac{h}{2}\right)^2+\nabla^2 w_2\left(\frac{h}{2}\right)^3+\nabla^2 w_3\left(\frac{h}{2}\right)^4+\right. \quad (19c)$$
$$\left.\nabla^2 w_4\left(\frac{h}{2}\right)^5+\nabla^2 w_5\left(\frac{h}{2}\right)^6+\nabla^2 w_6\left(\frac{h}{2}\right)^7\right)=0$$

$$\delta w_4 : \frac{\partial H_{xz}}{\partial x}+\frac{\partial H_{yz}}{\partial y}-3P_{zz}+q_z\left(\frac{h}{2}\right)^3-k_w\left(w_1\left(\frac{h}{2}\right)^3+w_2\left(\frac{h}{2}\right)^4+w_3\left(\frac{h}{2}\right)^5\right.$$
$$\left.+w_4\left(\frac{h}{2}\right)^6+w_5\left(\frac{h}{2}\right)^7+w_6\left(\frac{h}{2}\right)^8\right)+k_p\left(\nabla^2 w_1\left(\frac{h}{2}\right)^3+\nabla^2 w_2\left(\frac{h}{2}\right)^4+\nabla^2 w_3\left(\frac{h}{2}\right)^5\right. \quad (19d)$$
$$\left.+\nabla^2 w_4\left(\frac{h}{2}\right)^6+\nabla^2 w_5\left(\frac{h}{2}\right)^7+\nabla^2 w_6\left(\frac{h}{2}\right)^8\right)=0$$

$$\delta w_5 : \frac{\partial Y_{xz}}{\partial x}+\frac{\partial Y_{yz}}{\partial y}-4H_{zz}+q_z\left(\frac{h}{2}\right)^4-k_w\left(w_1\left(\frac{h}{2}\right)^4+w_2\left(\frac{h}{2}\right)^5+w_3\left(\frac{h}{2}\right)^6\right.$$
$$\left.+w_4\left(\frac{h}{2}\right)^7+w_5\left(\frac{h}{2}\right)^8+w_6\left(\frac{h}{2}\right)^9\right)+k_p\left(\nabla^2 w_1\left(\frac{h}{2}\right)^4+\nabla^2 w_2\left(\frac{h}{2}\right)^5+\nabla^2 w_3\left(\frac{h}{2}\right)^6\right. \quad (19e)$$
$$\left.+\nabla^2 w_4\left(\frac{h}{2}\right)^7+\nabla^2 w_5\left(\frac{h}{2}\right)^8+\nabla^2 w_6\left(\frac{h}{2}\right)^9\right)=0$$

$$\delta w_6 : \frac{\partial S_{xz}}{\partial x}+\frac{\partial S_{yz}}{\partial y}-5Y_{zz}+q_z\left(\frac{h}{2}\right)^5-k_w\left(w_1\left(\frac{h}{2}\right)^5+w_2\left(\frac{h}{2}\right)^6+w_3\left(\frac{h}{2}\right)^7+\right.$$
$$\left.w_4\left(\frac{h}{2}\right)^8+w_5\left(\frac{h}{2}\right)^9+w_6\left(\frac{h}{2}\right)^{10}\right)+k_p\left(\nabla^2 w_1\left(\frac{h}{2}\right)^5+\nabla^2 w_2\left(\frac{h}{2}\right)^6+\nabla^2 w_3\left(\frac{h}{2}\right)^7+\right. \quad (19f)$$
$$\left.\nabla^2 w_4\left(\frac{h}{2}\right)^8+\nabla^2 w_5\left(\frac{h}{2}\right)^9+\nabla^2 w_6\left(\frac{h}{2}\right)^{10}\right)=0$$

As far as the Eringen differential nonlocal model is concerned, the following formulation can be employed in terms of the stress resultants, where we adopt the superscript L to define the local stress and the superscript *NL* stands for the nonlocality,

$$\begin{cases}\left(1-\mu\nabla^2\right)\sigma_{ij}^{NL}=\sigma_{ij}^{L}\\ \left(1-\mu\nabla^2\right)\left(N_{ij}^{NL},M_{ij}^{NL},P_{ij}^{NL},H_{ij}^{NL},Y_{ij}^{NL},S_{ij}^{NL}\right)=N_{ij}^{L},M_{ij}^{L},P_{ij}^{L},H_{ij}^{L},Y_{ij}^{L},S_{ij}^{L}\end{cases} \tag{20}$$
$$\left(i,j=xx,yy,zz,xy,xz,yz\right)\qquad \mu=\left(e_0 a\right)^2$$

In Equation (20), μ represents the small scale usually named as nonlocal parameter; e_0 depends on the type of material and the parameter a is a length scale [4]. In addition, the local stress resultants can be converted into the nonlocal ones by considering the effect of the nonlocal parameter μ on the governing equations. Based on Equation (20) which relates the nonlocal and local stress resultants, after a long mathematical manipulation, here not reported for the sake of brevity, the governing Equations (17-19) can be converted into the following final form

$$\delta u_1:\frac{\partial N_{xx}}{\partial x}+\frac{\partial N_{xy}}{\partial y}=0 \tag{21a}$$

$$\delta u_2:\frac{\partial M_{xx}}{\partial x}+\frac{\partial M_{xy}}{\partial y}-N_{xz}=0 \tag{21b}$$

$$\delta u_3:\frac{\partial P_{xx}}{\partial x}+\frac{\partial P_{xy}}{\partial y}-2M_{xz}=0 \tag{21c}$$

$$\delta u_4:\frac{\partial H_{xx}}{\partial x}+\frac{\partial H_{xy}}{\partial y}-3P_{xz}=0 \tag{21d}$$

$$\delta u_5:\frac{\partial Y_{xx}}{\partial x}+\frac{\partial Y_{xy}}{\partial y}-4H_{xz}=0 \tag{21e}$$

$$\delta u_6:\frac{\partial S_{xx}}{\partial x}+\frac{\partial S_{xy}}{\partial y}-5Y_{xz}=0 \tag{21f}$$

$$\delta v_1:\frac{\partial N_{yy}}{\partial y}+\frac{\partial N_{xy}}{\partial x}=0 \tag{22a}$$

$$\delta v_2:\frac{\partial M_{yy}}{\partial y}+\frac{\partial M_{xy}}{\partial x}-N_{yz}=0 \tag{22b}$$

$$\delta v_3:\frac{\partial P_{yy}}{\partial y}+\frac{\partial P_{xy}}{\partial x}-2M_{yz}=0 \tag{22c}$$

$$\delta v_4:\frac{\partial H_{yy}}{\partial y}+\frac{\partial H_{xy}}{\partial x}-3P_{yz}=0 \tag{22d}$$

$$\begin{aligned}\delta w_6:&\frac{\partial S_{xz}}{\partial x}+\frac{\partial S_{yz}}{\partial y}-5Y_{zz}+\left(1-\mu\nabla^2\right)\left(q_z\left(\frac{h}{2}\right)^5-k_w\left(w_1\left(\frac{h}{2}\right)^5+w_2\left(\frac{h}{2}\right)^6+\right.\right.\\ &w_3\left(\frac{h}{2}\right)^7+w_4\left(\frac{h}{2}\right)^8+w_5\left(\frac{h}{2}\right)^9+w_6\left(\frac{h}{2}\right)^{10}\Big)+k_p\left(\nabla^2 w_1\left(\frac{h}{2}\right)^5+\nabla^2 w_2\left(\frac{h}{2}\right)^6+\right.\\ &\left.\left.\nabla^2 w_3\left(\frac{h}{2}\right)^7+\nabla^2 w_4\left(\frac{h}{2}\right)^8+\nabla^2 w_5\left(\frac{h}{2}\right)^9+\nabla^2 w_6\left(\frac{h}{2}\right)^{10}\right)\right)=0\end{aligned} \tag{22e}$$

$$\delta w_5 : \frac{\partial Y_{xz}}{\partial x} + \frac{\partial Y_{yz}}{\partial y} - 4H_{zz} + \left(1 - \mu\nabla^2\right)\left(q_z \left(\frac{h}{2}\right)^4 - k_w \left(w_1 \left(\frac{h}{2}\right)^4 + w_2 \left(\frac{h}{2}\right)^5 + \right.\right.$$
$$\left. w_3 \left(\frac{h}{2}\right)^6 + w_4 \left(\frac{h}{2}\right)^7 + w_5 \left(\frac{h}{2}\right)^8 + w_6 \left(\frac{h}{2}\right)^9 \right) + k_p \left(\nabla^2 w_1 \left(\frac{h}{2}\right)^4 + \nabla^2 w_2 \left(\frac{h}{2}\right)^5 + \right. \quad (22f)$$
$$\left.\left. \nabla^2 w_3 \left(\frac{h}{2}\right)^6 + \nabla^2 w_4 \left(\frac{h}{2}\right)^7 + \nabla^2 w_5 \left(\frac{h}{2}\right)^8 + \nabla^2 w_6 \left(\frac{h}{2}\right)^9 \right)\right) = 0$$

$$\delta w_1 : \frac{\partial N_{xz}}{\partial x} + \frac{\partial N_{yz}}{\partial y} + \left(1 - \mu\nabla^2\right)\left(q_z - k_w \left(w_1 + w_2 \left(\frac{h}{2}\right) + w_3 \left(\frac{h}{2}\right)^2 + \right.\right.$$
$$\left. w_4 \left(\frac{h}{2}\right)^3 + w_5 \left(\frac{h}{2}\right)^4 + w_6 \left(\frac{h}{2}\right)^5 \right) + k_p \left(\nabla^2 w_1 + \nabla^2 w_2 \left(\frac{h}{2}\right) + \nabla^2 w_3 \left(\frac{h}{2}\right)^2 + \quad (23a)$$
$$\left.\left. \nabla^2 w_4 \left(\frac{h}{2}\right)^3 + \nabla^2 w_5 \left(\frac{h}{2}\right)^4 + \nabla^2 w_6 \left(\frac{h}{2}\right)^5 \right)\right) = 0$$

$$\delta w_2 : \frac{\partial M_{xz}}{\partial x} + \frac{\partial M_{yz}}{\partial y} - N_{zz} + \left(1 - \mu\nabla^2\right)\left(q_z \left(\frac{h}{2}\right) - k_w \left(w_1 \left(\frac{h}{2}\right) + w_2 \left(\frac{h}{2}\right)^2 + \right.\right.$$
$$\left. w_3 \left(\frac{h}{2}\right)^3 + w_4 \left(\frac{h}{2}\right)^4 + w_5 \left(\frac{h}{2}\right)^5 + w_6 \left(\frac{h}{2}\right)^6 \right) + k_p \left(\nabla^2 w_1 \left(\frac{h}{2}\right) + \nabla^2 w_2 \left(\frac{h}{2}\right)^2 + \quad (23b)$$
$$\left.\left. \nabla^2 w_3 \left(\frac{h}{2}\right)^3 + \nabla^2 w_4 \left(\frac{h}{2}\right)^4 + \nabla^2 w_5 \left(\frac{h}{2}\right)^5 + \nabla^2 w_6 \left(\frac{h}{2}\right)^6 \right)\right) = 0$$

$$\delta w_3 : \frac{\partial P_{xz}}{\partial x} + \frac{\partial P_{yz}}{\partial y} - 2M_{zz} + \left(1 - \mu\nabla^2\right)\left(q_z \left(\frac{h}{2}\right)^2 - k_w \left(w_1 \left(\frac{h}{2}\right)^2 + w_2 \left(\frac{h}{2}\right)^3 + \right.\right.$$
$$\left. w_3 \left(\frac{h}{2}\right)^4 + w_4 \left(\frac{h}{2}\right)^5 + w_5 \left(\frac{h}{2}\right)^6 + w_6 \left(\frac{h}{2}\right)^7 \right) + k_p \left(\nabla^2 w_1 \left(\frac{h}{2}\right)^2 + \nabla^2 w_2 \left(\frac{h}{2}\right)^3 + \quad (23c)$$
$$\left.\left. \nabla^2 w_3 \left(\frac{h}{2}\right)^4 + \nabla^2 w_4 \left(\frac{h}{2}\right)^5 + \nabla^2 w_5 \left(\frac{h}{2}\right)^6 + \nabla^2 w_6 \left(\frac{h}{2}\right)^7 \right)\right) = 0$$

$$\delta w_4 : \frac{\partial H_{xz}}{\partial x} + \frac{\partial H_{yz}}{\partial y} - 3P_{zz} + \left(1 - \mu\nabla^2\right)\left(q_z \left(\frac{h}{2}\right)^3 - k_w \left(w_1 \left(\frac{h}{2}\right)^3 + w_2 \left(\frac{h}{2}\right)^4 + \right.\right.$$
$$\left. w_3 \left(\frac{h}{2}\right)^5 + w_4 \left(\frac{h}{2}\right)^6 + w_5 \left(\frac{h}{2}\right)^7 + w_6 \left(\frac{h}{2}\right)^8 \right) + k_p \left(\nabla^2 w_1 \left(\frac{h}{2}\right)^3 + \nabla^2 w_2 \left(\frac{h}{2}\right)^4 + \quad (23d)$$
$$\left.\left. \nabla^2 w_3 \left(\frac{h}{2}\right)^5 + \nabla^2 w_4 \left(\frac{h}{2}\right)^6 + \nabla^2 w_5 \left(\frac{h}{2}\right)^7 + \nabla^2 w_6 \left(\frac{h}{2}\right)^8 \right)\right) = 0$$

$$\delta w_5 : \frac{\partial Y_{xz}}{\partial x} + \frac{\partial Y_{yz}}{\partial y} - 4H_{zz} + \left(1 - \mu\nabla^2\right)\left(q_z \left(\frac{h}{2}\right)^4 - k_w \left(w_1 \left(\frac{h}{2}\right)^4 + w_2 \left(\frac{h}{2}\right)^5 + \right.\right.$$
$$\left. w_3 \left(\frac{h}{2}\right)^6 + w_4 \left(\frac{h}{2}\right)^7 + w_5 \left(\frac{h}{2}\right)^8 + w_6 \left(\frac{h}{2}\right)^9 \right) + k_p \left(\nabla^2 w_1 \left(\frac{h}{2}\right)^4 + \nabla^2 w_2 \left(\frac{h}{2}\right)^5 + \quad (23e)$$
$$\left.\left. \nabla^2 w_3 \left(\frac{h}{2}\right)^6 + \nabla^2 w_4 \left(\frac{h}{2}\right)^7 + \nabla^2 w_5 \left(\frac{h}{2}\right)^8 + \nabla^2 w_6 \left(\frac{h}{2}\right)^9 \right)\right) = 0$$

$$\delta w_6 : \frac{\partial S_{xz}}{\partial x}+\frac{\partial S_{yz}}{\partial y}-5Y_{zz}+\left(1-\mu\nabla^2\right)\Bigg(q_z\left(\frac{h}{2}\right)^5-k_w\Bigg(w_1\left(\frac{h}{2}\right)^5+w_2\left(\frac{h}{2}\right)^6+$$
$$w_3\left(\frac{h}{2}\right)^7+w_4\left(\frac{h}{2}\right)^8+w_5\left(\frac{h}{2}\right)^9+w_6\left(\frac{h}{2}\right)^{10}\Bigg)+k_p\Bigg(\nabla^2 w_1\left(\frac{h}{2}\right)^5+\nabla^2 w_2\left(\frac{h}{2}\right)^6+ \tag{23f}$$
$$\nabla^2 w_3\left(\frac{h}{2}\right)^7+\nabla^2 w_4\left(\frac{h}{2}\right)^8+\nabla^2 w_5\left(\frac{h}{2}\right)^9+\nabla^2 w_6\left(\frac{h}{2}\right)^{10}\Bigg)\Bigg)=0$$

The numerical analysis of the thermoelastic response considers several boundary conditions at $y=0, x=0, y=L_y, x=L_x$. For example, CFCF boundary conditions means that the plate is clamped at $y=0, L_y$ and free in $x=0, L_x$. Here below a detailed definition of the boundary conditions are demonstrated

1- Clamped (C)

$$\begin{cases} u_i\ (i=1...6)=0 \ \ x=0,L_x\,; y=0,L_y \\ v_i\ (i=1...6)=0 \ \ x=0,L_x\,; y=0,L_y \\ w_i\ (i=1...6)=0 \ \ x=0,L_x\,; y=0,L_y \end{cases} \tag{24}$$

2- Free (F)

$$\begin{aligned} x=0,L_x\ :\ & \begin{cases} N_{xx}=N_{xy}=M_{xy}=P_{xy}=H_{xy}=Y_{xy}=S_{xy}=0 \\ M_{xx}=P_{xx}=H_{xx}=Y_{xx}=S_{xx}=0 \\ N_{xz}=M_{xz}=P_{xz}=H_{xz}=Y_{xz}=S_{xz}=0 \end{cases} \\ y=0,L_y\ :\ & \begin{cases} N_{yy}=N_{xy}=M_{xy}=P_{xy}=H_{xy}=Y_{xy}=S_{xy}=0 \\ M_{yy}=P_{yy}=H_{yy}=Y_{yy}=S_{yy}=0 \\ N_{yz}=M_{yz}=P_{yz}=H_{yz}=Y_{yz}=S_{yz}=0 \end{cases} \end{aligned} \tag{25}$$

3- Simply-supported

$$\begin{aligned} x=0,L_x\ :\ & \begin{cases} u_1=v_1=w_1=w_2=w_3=w_4=w_5=w_6=0 \\ N_{xx}=N_{xy}=M_{xy}=N_{xz}=M_{xz}=0 \\ M_{xx}=P_{xx}=H_{xx}=Y_{xx}=S_{xx}=0 \end{cases} \\ y=0,L_y\ :\ & \begin{cases} u_1=v_1=w_1=w_2=w_3=w_4=w_5=w_6=0 \\ M_{yy}=P_{yy}=H_{yy}=Y_{yy}=S_{yy}=0 \\ N_{yy}=N_{xy}=M_{xy}=N_{yz}=M_{yz}=0 \end{cases} \end{aligned} \tag{26}$$

3. Semi-Analytical Polynomial solution

In this work we propose a semi-analytical polynomial solution method (SAPM) to solve the system of partial differential equations with any boundary conditions, due to its relative simplicity and efficiency. According to the proposed method, a polynomial expression of the kinematic unknowns ($u_i, v_i, w_i\ (i=1...6)$) is introduced as follows

$$u_i = \sum_{k=1}^{N}\sum_{t=1}^{M} a_{\left(k+t-\left(1-(k-1)(M-1)\right)+(i-1)\times M\cdot N\right)} x^{(k-1)} y^{(t-1)} \qquad (i=1..6)$$

$$v_i = \sum_{k=1}^{N}\sum_{t=1}^{M} a_{\left(k+t-\left(1-(k-1)(M-1)\right)+(i-1)\times M\cdot N+6\times M\cdot N\right)} x^{(k-1)} y^{(t-1)} \qquad (i=1..6) \qquad (27)$$

$$w_i = \sum_{k=1}^{N}\sum_{t=1}^{M} a_{\left(k+t-\left(1-(k-1)(M-1)\right)+(i-1)\times M\cdot N+12\times M\cdot N\right)} x^{(k-1)} y^{(t-1)} \qquad (i=1..6)$$

Please, note that the kinematic variables are a_i, for a total number of unknowns equal to $18\times M\times N$, where N, M refers to discretization in the x- and y-direction, respectively. More specifically, $2M+2N-4$ unknowns follow the boundary conditions of the problem, whereas $(M-2)(N-2)$ unknowns must be a function of the obtained basic equations (with $(M-2)(N-2)=M\times N-2M-2N+4$).

Now, if the total number of equations obtained from boundary conditions ($2M+2N-4$) are summed up with the governing relations of the problem ($(M-2)(N-2)$), we obtain $M\times N$ equations for each kinematic unknown u_i. Totally, there are 18 basic equations and 18 variables, such that a total number of $18\times M\times N$ equations is achieved. A Newton-Raphson scheme is adopted to solve numerically this system of algebraic, and determine the functions u_i, v_i, w_i $(i=1...6)$, which define the structural deflection of the plate.

4. Numerical examples

Within a large numerical investigation of the problem, first, we validate the results based on our formulation with predictions based on the third-order shear deformation theory (TSDT), and computations from the ABAQUS code (see Table 1). The following dimensions and mechanical properties are assumed for the plate in Table 1

$$L_x = 1\text{m};\ L_y = 2\text{m};\ E = 1.9\times 10^{11}\ \text{Pa};\ \nu = 0.29;\ q_z = 0.1\text{GPa}$$

Based on a comparative evaluation, the good agreement between our results and those ones from ABAQUS confirms the accuracy of our proposed formulation. However, some remarkable differences between our results and the TSDT-based results can be noticed for higher values of thickness ($h = 0.5\text{m}$). The TSDT, indeed, ignores the strain changes along the thickness, and the amount of ε_z is equal to zero, accordingly. In other words, the applied SAPM in combination with the proposed displacement field (Equations (3a-c)) gives appropriate results for moderately thick rectangular plates. Two further comparative evaluations are presented in Tables 2 and 3 whose results are compared with the available literature. In Table 2, it is assumed:

$$E_x = 18.7\times 10^6;\ E_y = 1.3\times 10^6;\ G_{xy} = 0.6\times 10^6;$$

$$L_x = 9.4\text{nm};\ L_y = 7.75\text{nm};\ h = 0.0624\text{nm};\ \nu_{\text{xy}} = 0.3;\ w^* = \frac{w}{L_x}$$

where as in Table 3, the following data are considered

$$E_x = 2.434\times 10^6;\ E_y = 2.473\times 10^6;\ G_{xy} = 1.039\times 10^6;$$

$$L_x = 9.519\text{nm};\ L_y = 4.844\text{nm};\ h = 0.129\text{nm};\ \nu_{\text{xy}} = 0.197$$

Both Tables 2 and 3 confirm the efficiency and accuracy of our proposed method. Thus, the results obtained in this paper can be used with high level of accuracy especially for moderately thick plates for which common plate theories such as CLPT, FSDT and TSDT could not give appropriate results. In line with the previous results, Figure 3 examines the rate of convergence of results when applying a SAPM solving procedure. For this scope, the double assumption of CCCC and CFCF boundary conditions is done. In this case, the plate features the following geometry and mechanical parameters:

A dimensionless thickness-to-length ratio is considered to show the behavior of a thick sheet. In the following analysis, a graphene material is considered. The graphs are plotted across the thickness of the sheet, for a suitable representation of the 3D elasticity analysis. Differently from a two-dimensional elasticity approach for which the maximum deflection occurs at the center of the thickness, according to our formulation, the neutral axis shifts toward the upper (+z) levels and yields the maximum deflection in the upper layers.

Based on a comparative evaluation of plots in Figures 3a and b, the rate of convergence is smoother for more rigid boundary conditions, although, the results are generally convergent at nine points for both boundary conditions. A sharp rise can be noticed, for a CCCC, when a 7x7 and a 9x9 grid distribution is applied. Since the three-dimensional analysis means a change in thickness of the sheet, the dimensionless deflection at the upper surface is higher than the one at the lower surface. This is line with the through-the-thickness compression induced at the top surface by the external loading, which is added to the overall deflection of the sheet.

Figure 4 compares the deflection response, as provided by the fifth-order expansion in Equations (3a-c), or a third-order three-dimensional displacement field defined below as.

$$\begin{aligned} U(x,y,z) &= u_1(x,y) + z u_2(x,y) + z^2 u_3(x,y) + z^3 u_4(x,y) \\ V(x,y,z) &= v_1(x,y) + z v_2(x,y) + z^2 v_3(x,y) + z^3 v_4(x,y) \\ W(x,y,z) &= w_1(x,y) + z w_2(x,y) + z^2 w_3(x,y) + z^3 w_4(x,y) \end{aligned} \tag{28}$$

Based on Figure 4, it is worth noticing the fast convergence of the solution for a third-order expansion, at least for a rigid CCCC boundary condition (see Figure 4a). In this case, indeed, the third-order-based results do not differ significantly from the ones provided by a fifth order expansion, whereas more flexible CFCF boundary conditions increase significantly the discrepancies between the two approaches, such that a third-order expansion would be no longer sufficient to guarantee accurate results. This means that the selection of the order of expansion is strictly related to the level of constraint of the plate. To study the possible effect of the grading index g in a FGM, Figure 5 plots the kinematic response of a square nanoplate with length $L_x = L_y = 3\text{nm}$, thickness $h = 1\text{nm}$, and the following mechanical properties: $E_m = 201\text{GPa}; E_c = 602\text{GPa}$; $\nu = 0.25$; $q_z = 1\text{GPa}$; $e_0 a = 0$ (see Table 4), under the double assumption of CCCC and FCFC boundary conditions. As visible in Figures 5a and b, the deflection of the plate increases monotonically for increasing grading indexes, with a similar response for both boundary conditions. In both cases, a very fast increase of the deflection can be observed moving from $g = 0$ up to $g = 5$, whereas very large values of g reduce their effect on the global deformability of the nanoplate. Please, note that, the limit cases of zero index or infinite index refer to the pure "ceramic" or "metal" material, for which the highest and lowest structural stiffness is enriched, respectively, due to the higher Young's modulus featuring the ceramic material. Please, note also that for FGMs, the top surface of the sheet features the maximum deflection, due to its higher compression and thickness reduction compared to the other layers.

Figure 6 plots the effect of the dimensionless ratio L_x/h on the structural deflection of a thick plate, according to the proposed three-dimensional elasticity theory. For a moderately thick sheet with $L_x/h=2$, the maximum increase of deflection is observed at the top layers of the plate. For thinner plates, instead, the reduction in the thickness becomes even more unrecognizable and the deflection at upper and lower layers (i.e. for $z^*=-0.5$ and $z^*=0.5$) maintains almost constant. This emphasizes the importance of adopting a three-dimensional elasticity theory for moderately thick plates. For the sake of completeness, in Figure 7 we provide a comparative evaluation of the kinematic response of a thick plate, according to the current three-dimensional elasticity and the classical TSDT. The properties of the plate are assumed as follows:

$$L_x = L_y = 2\text{nm};\ h = 1\text{nm};\ E_m = 201\text{GPa};\ E_c = 602\text{GPa};\ \nu = 0.25;$$
$$q_z = 9\text{GPa};\ k_w = 1.13\text{GPa/nm};\ k_p = 1.13\text{Pa}\times\text{m}$$

As expectable, the TSDT provides a constant deflection along the whole thickness domain of the thick plate, whereby the real graduation in the kinematic response along the thickness can be captured only when applying our proposed three-dimensional theory. Another interesting aspect is related to the effect of the nonlocal parameter on the structural response, which is more pronounced in a TSDT compared to our proposed 3D elasticity theory. This is probably due to the nonlocal effect in the direction of thickness ($\partial^2/\partial z^2$) which is ignored in plate theories.

Two different values of the nonlocal coefficient are assumed, namely $e_0a=1nm$; whereas the temperature variation is increased from a null value up to 400°C. As visible in Figure 8, the increase in temperature leads to an increased or decreased deflection for positive or negative layers along the thickness, respectively. According to the 3D elastic theory, even in absence of a transverse mechanical load, we can capture the structural deflection related to the only temperature increase, otherwise not visible through classical bi-dimensional plate theories (see, Ref. [4]). This confirms the importance of using a three-dimensional elasticity theory and the efficiency of our proposed formulation. Another key aspect is the sensitivity of the thermoelastic response to the nonlocal coefficient, where an increased nonlocal parameter leads to an increased stiffness of the material and a gradual reduction in the plate deflection, for the same fixed temperature variation. In addition, the displacement field for points located at the middle surface (i.e. for $z=0$) is visibly unaffected by the temperature variation, since it maintains exactly the same for different ΔT and a given value of the nonlocal parameter. Please, note that the nanostructure is initially at a room temperature of 27 °C, which is here assumed as reference temperature for further variations within the parametric analysis.

Figure 9 also plots the effect of the environmental humidity on the modeled FGM sheet. To this end, moisture variations are considered up to a maximum percentage of 40%. By comparison between Figures 8 and 9, the structural deflection is much more affected by moisture than temperature, in line with findings by Malikan and Nguyen [31].

A small increase in the humidity vary significantly the deformability of the nanostructure, with a general increase or decrease of the displacement field for layers located at negative or positive z^*-coordinates, respectively. It is also interesting to note that for a low level of humidity, the $w-z^*$ curves shift downwards for an increased nonlocality, which means that the stiffness increases proportionally along the thickness. An interesting comparison between results coming from our formulation and a classical TSDT plate theory is shown in Figure 10, for different temperature variations. Based on the plots of Figure 10, it is worth observing that the TSDT is quite inaccurate for thick or moderately thick plates, since it yields constant displacements independently of the z^*-coordinate and the surrounding temperature. A different monotone variation is predicted by the proposed three-dimensional theory along the thickness.

A further parametric investigation accounts for the possible effect of uneven or even porosities on the structural response of FGM nanoplates, as visible in Figures 11a and b, respectively, where we assume the following geometrical and mechanical parameters:

$$L_x = L_y = 4\text{nm};\ h = 1\text{nm};\ E_m = 201\text{GPa};\ E_c = 602\text{GPa};\ g = 10;\ \nu = 0.25;\ q_z = 1\text{GPa}$$

$$k_p = 1.13\text{Pa}\times\text{m};\ \alpha_m = 12\times10^{-6}\left(\frac{1}{K^\circ}\right);\ \alpha_c = 5\times10^{-6}\left(\frac{1}{K^\circ}\right);\ \Delta T = 200\text{C}^\text{o};\ \beta = 0.33$$

$$\Delta H = 0.1;\ k_w = 1.13\text{GPa/nm};\ \text{Boundaries: CCCC}$$

By comparing Figures 11a and b, it is clear that even porosities result in a weaker sheet [5]. In fact, the number of holes in the plate, due to the improper manufacturing process and errors, could weaken the material. This can be seen from the larger deflections in Figure 11b than those ones in Figure 11a. On the other hand, in Figure 11a it can be seen that whenever the nonlocal parameter is larger, the effect of porosity on the results becomes smaller. In addition, for both porosity distributions, the through-the-thickness deflection response is almost linear, while maintaining the same slope.

For FGM sheets immersed within an elastic foundation, a further study aims at analyzing the effect of the Winkler or Pasternak coefficients to the overall deflection (see Figures 12a and b). In order to check for the accuracy of the results, the present elasticity theory is compared to the TSDT, for different dimensionless L_x/h parameters. More in detail, for thinner plates with $L_x/h = 4$, static deflections provided by the present theory and the TSDT are perfectly the same, at least, for positive layers. This is not still true for thicker plates ($L_x/h = 2$), where both positive and negative layers along the thickness feature quite different results depending on whether a 3D-based theory or a TSDT is applied. Whenever the plate thickness is increased, possible discrepancies between the results based on the two different approaches gradually increase. Moreover, by comparing Figures 12a and b, a variation in the stiffness coefficient for a Winkler foundation affects more significantly the static deflection than the one related to a Pasternak foundation, for the same fixed geometry of the structure and nonlocal parameter.

5. Conclusions

This work proposes a novel three-dimensional elasticity theory to study the coupled thermo-hygro-mechanical behavior of FG nanostructures. The proposed approach requires an easy process to be solved, and investigates the small-scale effects in nanostructures, when combined with the Eringen nonlocal theory. The nanoplates studied herein, are assumed to lie on a two-parameter elastic base, and are immersed in a coupled thermal and moisture environment. Possible effects of the structural response account for the presence of different porosity distributions within the nanomaterial, as typically occurs during an actual manufacturing process. The problem is solved by means of a semi-analytical polynomial method (SAPM), which is validated against the available literature, while estimating its accuracy. Among a large parametric study, the following conclusions can be summarized as follows:

- For two-dimensional elasticity analyses, the through-the-thickness deflection is constant, whereas the proposed three-dimensional approach estimates any possible variation in the kinematic response for both negative and positive layers. In most cases, the maximum deflection is enriched at the top surface of the plate, because of its compressive reduction due to the external loading condition. As a common definition, many scholars assume the maximum deflection occurs in the mid-plan of the thickness. But, considering deflections through the thickness confirms that this is not always true. The maximum deflections occur in upper surfaces of the plate because of both transverse deflections and thickness variations.

- The sensitivity of the deflection response to the nonlocal parameter for the present theory is less pronounced than the one based on the TSDT for thick plates, because of the use of three-dimensional Laplacian operators for the nonlocal relations.

- Plate theories fail for thick and moderately thick plates, and they become totally inaccurate, if compared to the proposed three-dimensional approach, especially for more complex coupled problems accounting for different thermo-hygro-mechanical conditions.

References

[1] Shinohara, Y. *Handbook of Advanced Ceramics* (Second Edition), Elsevier, 2013; pp. 1258, https://doi.org/10.1016/C2010-0-66261-4.

[2] Ichikawa, K. *Functionally Graded Materials in the 21st Century*, Springer, 2001; pp. XVI, 242, doi. 10.1007/978-1-4615-4373-2.

[3] Kompiš, V. *Composites with Micro- and Nano-Structure*, Springer, 2008; pp. X, 302, doi: 10.1007/978-1-4020-6975-8.

[4] Dastjerdi, Sh.; Akgöz, B. New static and dynamic analyses of macro and nano FGM plates using exact three-dimensional elasticity in thermal environment. *Compos Struct* **2018**, 192, 626-641.

[5] Malikan, M.; Tornabene, F.; Dimitri, R. Nonlocal three-dimensional theory of elasticity for buckling behavior of functionally graded porous nanoplates using volume integrals. *Mater Res Express* **2018**, 5, 095006.

[6] Ansari, R.; Shahabodini, A.; Faghih Shojaei, M. Nonlocal three-dimensional theory of elasticity with application to free vibration of functionally graded nanoplates on elastic foundations. *Physica E: Low-dim Syst and Nanostruct* **2016**, 76, 70-81.

[7] Malikan, M.; Dimitri, R.; Tornabene, F. Transient response of oscillated carbon nanotubes with an internal and external damping. *Compos Part B: Eng* **2019**, 15, 198-205.

[8] Brischetto, S. Exact three-dimensional static analysis of single- and multi-layered plates and shells. *Compos Part B: Eng* **2017**, 119, 230-252.

[9] Ansari, R.; Faghih Shojaei, M.; Shahabodini, A.; Bazdid-Vahdati, M. Three-dimensional bending and vibration analysis of functionally graded nanoplates by a novel differential quadrature-based approach. *Compos Struct* **2015**, 131, 753-764.

[10] Tornabene, F.; Brischetto, S.; Fantuzzi, N.; Viola, E. Numerical and exact models for free vibration analysis of cylindrical and spherical shell panels. *Compos Part B: Eng* **2015**, 81, 231-250.

[11] Tornabene, F.; Fantuzzi, N.; Bacciocchi, M. The GDQ method for the free vibration analysis of arbitrarily shake laminated composite shells using a NURBS-based isogeometric approach. *Compos Struct* **2016**, 154, 190-218.

[12] Tornabene, F.; Brischetto, S.; Fantuzzi, N.; Bacciocchi, M. Boundary conditions in 2D numerical and 3D exact models for cylindrical bending analysis of functionally graded structures. *Shock and Vib* **2016**, 2373862.

[13] Tornabene, F.; Fantuzzi, N.; Bacciocchi, M. Higher-order structural theories for the static analysis of doubly-curved laminated composite panels reinforced by curvilinear fibers. *Thin Wall Struct* **2016**, 102, 222-245.

[14] Dastjerdi, Sh.; Akgöz, B.; Yazdanparast, L. A new approach for bending analysis of bilayer conical graphene panels considering nonlinear van der Waals force. *Compos Part B: Eng* **2018**, 150, 124-134.

[15] Dastjerdi, Sh.; Jabbarzadeh, M. Bending sector graphene sheet based on the elastic Winkler-Pasternak with the help of nonlocal elasticity theory using developed Kantorovich method. *J Simul and Analys of Novel Tech in Mech Eng* (*J Solid Mech in Eng*) **2014**, 7, 35-49.

[16] Dastjerdi, Sh.; Jabbarzadeh, M.; Tahani, M. Nonlinear bending analysis of sector graphene sheet embedded in elastic matrix based on nonlocal continuum mechanics. *Inter J Eng-Transactions B: App* **2015**, 28, 802-811.

[17] Dastjerdi, Sh.; Abbasi, M.; Yazdanparast, L. A new modified higher-order shear deformation theory for nonlinear analysis of macro-and nano-annular sector plates using the extended Kantorovich method in conjunction with SAPM. *Acta Mech* **2017**, 228, 3381-3401.

[18] Salehipour, H.; Nahvi, H.; Shahidi, A. R.; Mirdamadi, H. R. 3D elasticity analytical solution for bending of FG micro/nanoplates resting on elastic foundation using modified couple stress theory. *Appl Math Model* **2017**, 47, 174-188.
[19] Alibeigloo, A. Three dimensional coupled thermoelasticity solution of sandwich plate with FGM core under thermal shock. *Compos Struct* **2017**, 177, 96-103.
[20] Wang, Y.-Q.; Zu, J.-W. Vibration behaviors of functionally graded rectangular plates with porosities and moving in thermal environment. *Aerosp Sci and Technol* **2017**, 69, 550-562.
[21] Dastjerdi, Sh.; Lotfi, M.; Jabbarzadeh, M. The effect of vacant defect on bending analysis of graphene sheets based on the Mindlin nonlocal elasticity theory. *Compos Part B: Eng* **2016**, 98, 78-87.
[22] Dastjerdi, Sh.; Jabbarzadeh, M. Non-Local Thermo-Elastic Buckling Analysis of Multi-Layer Annular/Circular Nano-Plates Based on First and Third Order Shear Deformation Theories Using DQ Method. *J Solid Mech* **2016**, 8, 859-874.
[23] Dastjerdi, Sh.; Lotfi, M.; Jabbarzadeh, M. Nonlocal analysis of single and double-layered graphene cylindrical panels and nano-tubes under internal and external pressures considering thermal effects. *J Theor Appl Mech* **2017**, 55, 883-896.
[24] Malikan, M.; Jabbarzadeh, M.; Dastjerdi, Sh. Non-linear Static stability of bi-layer carbon nanosheets resting on an elastic matrix under various types of in-plane shearing loads in thermo-elasticity using nonlocal continuum. *Microsyst Technol* **2017**, 23, 2973-2991.
[25] Wang, Y.-Q. Electro-mechanical vibration analysis of functionally graded piezoelectric porous plates in the translation state. *Acta Astronaut* **2018**, 143, 263-271.
[26] Jouneghani, F. Z.; Dimitri, R.; Tornabene, F. Structural response of porous FG nanobeams under hygro-thermo-mechanical loadings. *Compos Part B: Eng* **2018**, 152, 71-78.
[27] Malikan, M.; Nguyen, V. B.; Tornabene, F. Damped forced vibration analysis of single-walled carbon nanotubes resting on viscoelastic foundation in thermal environment using nonlocal strain gradient theory. *Eng Sci and Tech, an Inter J* **2018**, 21, 778-786.
[28] Fares, M. E.; Elmarghany, M. Kh.; Atta, D.; Salem, M. G. Bending and free vibration of multilayered functionally graded doubly curved shells by an improved layerwise theory. *Compos Part B: Eng* **2018**, 154, 272-284.
[29] Sator, L.; Sladek, V.; Sladek, J. Bending of FGM plates under thermal load: Classical thermoelasticity analysis by a meshless method. *Compos Part B: Eng* **2018**, 146, 176-188.
[30] Malikan, M.; Nguyen, V. B.; Tornabene, F. Electromagnetic forced vibrations of composite nanoplates using nonlocal strain gradient theory. *Mater Res Express* **2018**, 5, 075031.
[31] Malikan, M., Nguyen, V. B. Buckling analysis of piezo-magnetoelectric nanoplates in hygrothermal environment based on a novel one variable plate theory combining with higher-order nonlocal strain gradient theory. *Physica E: Low-dim Syst and Nanostruct* **2018**, 102, 8-28.
[32] Malikan, M.; Dimitri, R.; Tornabene, F. Effect of sinusoidal corrugated geometries on the vibrational response of viscoelastic nanoplates. *Appl Sci* **2018**, 8, 1432.
[33] Sator, L.; Sladek, V.; Sladek, J. Analysis of coupling effects in FGM piezoelectric plates by a meshless method. *Compos Struct* **2020**, 244, 112256.
[34] Kumar, R.; Lal, A.; Singh, B. N.; Singh, J. Non-linear analysis of porous elastically supported FGM plate under various loading. *Compos Struct* **2020**, 233, 111721.
[35] Dastjerdi, S.; Akgöz, B.; Civalek, Ö. On the effect of viscoelasticity on behavior of gyroscopes. *Inter J Eng Sci* **2020**, 149, 103236.
[36] Malikan, M.; Eremeyev, V. A. A new hyperbolic-polynomial higher-order elasticity theory for mechanics of thick FGM beams with imperfection in the material composition. *Compos Struct* **2020**, 249, 112486.
[37] Karamanli, A.; Aydogdu, M. Bifurcation buckling conditions of FGM plates with different boundaries. *Compos Struct* **2020**, 245, 112325.
[38] Adhikari, B.; Dash, P.; Singh, B. N. Buckling analysis of porous FGM sandwich plates under various types nonuniform edge compression based on higher order shear deformation theory. *Compos Struct* **2020**, 251, 112597.
[39] Malikan, M.; Nguyen, V. B.; Dimitri, R.; Tornabene, F. Dynamic modeling of non-cylindrical curved viscoelastic single-walled carbon nanotubes based on the second gradient theory. *Mater Res Express* **2019**, 6, 075041.
[40] Malikan, M. Electro-mechanical shear buckling of piezoelectric nanoplate using modified couple stress theory based on simplified first order shear deformation theory. *Appl Math Model* **2017**, 48, 196-207.

[41] Liang, C.; Wang, Y. Q. A quasi-3D trigonometric shear deformation theory for wave propagation analysis of FGM sandwich plates with porosities resting on viscoelastic foundation. *Compos Struct* **2020**, 247, 112478
[42] Lomte Patil, Y. T.; Kant, T.; Desai, Y. M. Comparison of Three Dimensional Elasticity Solutions for Functionally Graded Plates. *Compos Struct* **2018**, 202, 424-435.
[43] Dastjerdi, Sh.; Jabbarzadeh, M. Nonlinear bending analysis of bilayer orthotropic graphene sheets resting on Winkler-Pasternak elastic foundation based on non-local continuum mechanics. *Compos Part B: Eng* **2016**, 87, 161-175.
[44] Dastjerdi, Sh.; Jabbarzadeh, M.; Aliabadi, S. Nonlinear static analysis of single layer annular/circular graphene sheets embedded in Winkler–Pasternak elastic matrix based on non-local theory of Eringen. *Ain Shams Eng J* **2016**, 7, 873-884.
[45] Dastjerdi, Sh.; Jabbarzadeh, M. Nonlocal Bending Analysis of Bilayer Annular/Circular Nano Plates Based on First Order Shear Deformation Theory. *J Solid Mech* **2016**, 8, 645-661.
[46] Dastjerdi, Sh.; Jabbarzadeh, M. Non-linear bending analysis of multi-layer orthotropic annular/circular graphene sheets embedded in elastic matrix in thermal environment based on non-local elasticity theory. *Appl Math Model* **2017**, 41, 83-101.
[47] Malikan, M.; Sadraee Far, M. N. Differential quadrature method for dynamic buckling of graphene sheet coupled by a viscoelastic medium using neperian frequency based on nonlocal elasticity theory. *J Appl and Comput Mech* **2018**, 4, 147-160.
[48] Karami, B.; Janghorban, M.; Tounsi, A. Nonlocal strain gradient 3D elasticity theory for anisotropic spherical nanoparticles. *Steel and Compos Struct* **2018**, 27, 201-216.
[49] She, G.-L.; Yuan, F.-G.; Ren, Y.-R.; Liu, H.-B.; Xiao, W.-Sh. Nonlinear bending and vibration analysis of functionally graded porous tubes via a nonlocal strain gradient theory. *Compos Struct* **2018**, 203, 614-623.
[50] Ahmed Hassan, A. H.; Kurgan, N. Bending analysis of thin FGM skew plate resting on Winkler elastic foundation using multi-term extended Kantorovich method. *Eng Sci Technol an Int J* **2020**, 23, 788-800.
[51] Dastjerdi, Sh.; Akgöz, B. On the statics of fullerene structures. *Int J Eng Sci* **2019**, 142, 125-144.
[52] Karami, B.; Shahsavari, D.; Janghorban, M; Dimitri, R.; Tornabene, F. Wave propagation of porous nanoshells. *Nanomaterials* **2019**, 9, 22.
[53] Rahmati, A. H.; Yang, S.; Bauer, S.; Sharma, P. Nonlinear bending deformation of soft electrets and prospects for engineering flexoelectricity and transverse (d_{31}) piezoelectricity. *Soft Matter* **2019**, 15, 127-148.
[54] Golmakani, M. E.; Rezatalab, J. Nonlinear bending analysis of orthotropic nanoscale plates in an elastic matrix based on nonlocal continuum mechanics. *Compos Struct* **2014**, 111, 85-97.
[55] Chen, W.; Shu, C.; He, W.; Zhong, T. The application of special matrix product to differential quadrature solution of geometrically nonlinear bending of orthotropic rectangular plates. *Comput & Struct* **2000**, 74, 65–76.
[56] Golmakani, M. E.; Sadraee Far, M. N. Nonlinear thermo-elastic bending behavior of graphene sheets embedded in an elastic medium based on nonlocal elasticity theory. *Comput and Math with App* **2016**, 72, 785-805.
[57] Golmakani, M. E.; Malikan, M.; Sadraee Far, M. N.; Majidi, H. R. Bending and buckling formulation of graphene sheets based on nonlocal simple first order shear deformation theory. *Mater Res Express* **2018**, 5, 065010.
[58] Yang, J.; Shen, H.-S. Vibration characteristics and transient response of shear-deformable functionally graded plates in thermal environments. *J Sound and Vib* **2002**, 255, 579-602.
[59] Ziaee, S. Small scale effect on linear vibration of buckled size-dependent FG nanobeams. *Ain Shams Eng J* **2015**, 6, 587-598.
[60] Zidi, M.; Tounsi, A.; Houari, M. S. A.; Adda Bedia, E. A.; Bég, O. A. Bending analysis of FGM plates under hygro-thermo-mechanical loading using a four variable refined plate theory. *Aerosp Sci and Technol* **2014**, 34, 24–34.
[61] Fan, Q.; Chai, Ch.; Wei, Q.; Yang, Y. The Mechanical and Electronic Properties of Carbon-Rich Silicon Carbide. *Materials* **2016**, 9, 333. doi:10.3390/ma9050333.

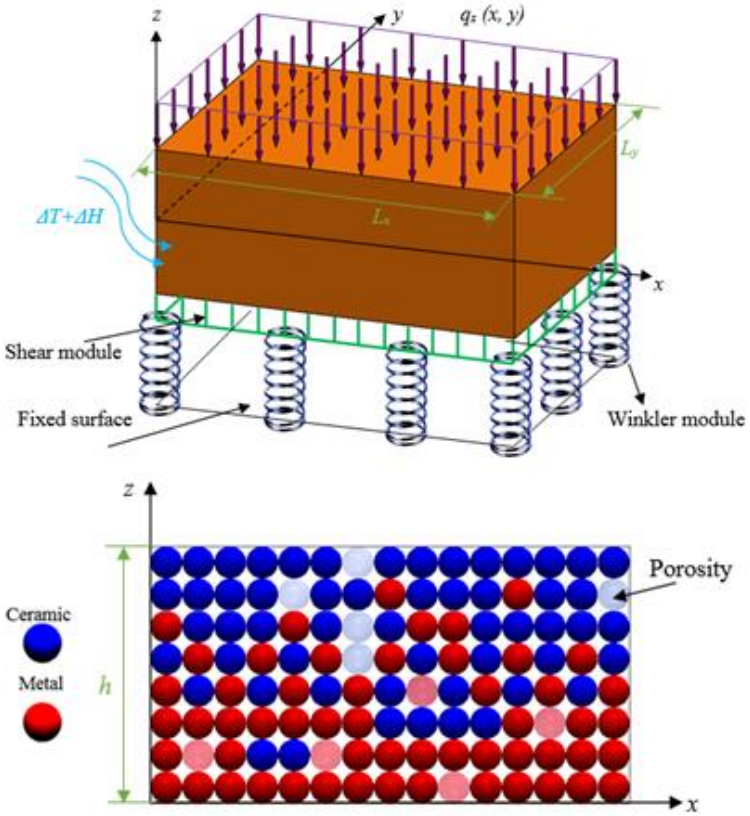

Figure 1. Moderately thick nanoporous FG rectangular plate in a hygro-thermal surround.

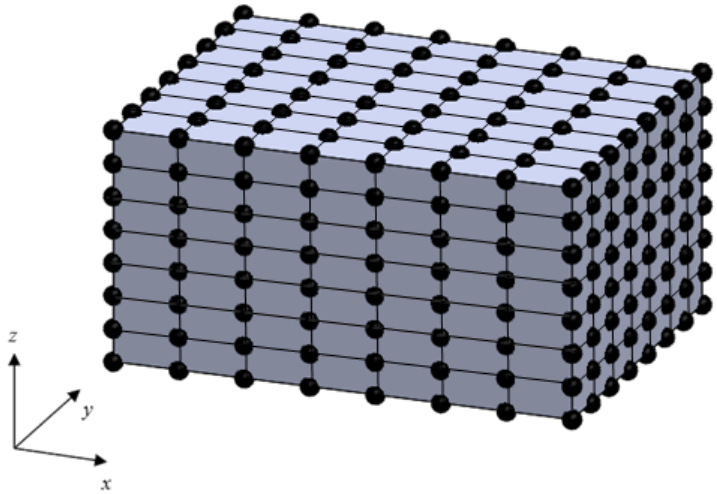

Figure 2. Grid points distribution within the 3D plate.

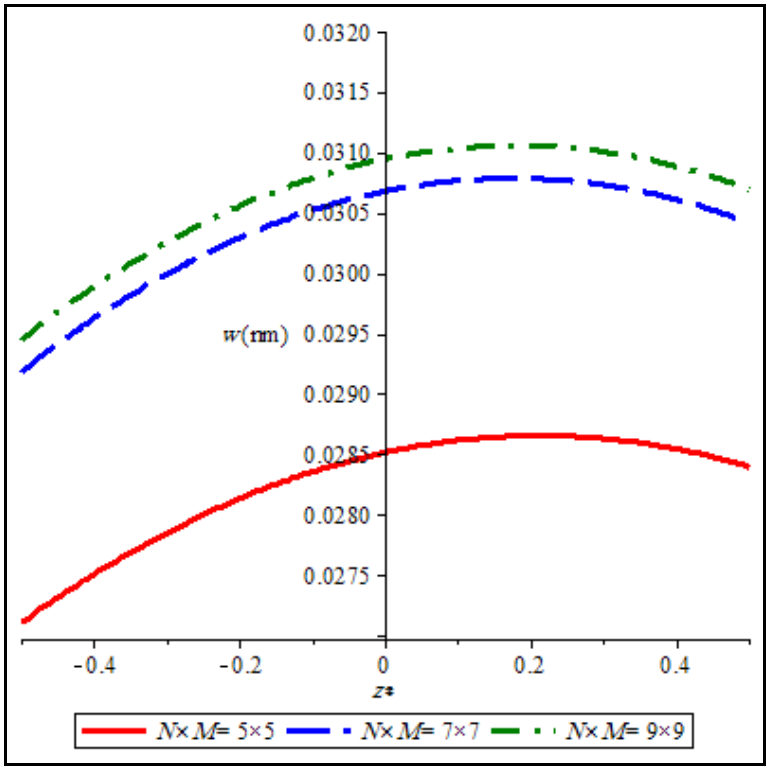

(a) CCCC boundary condition

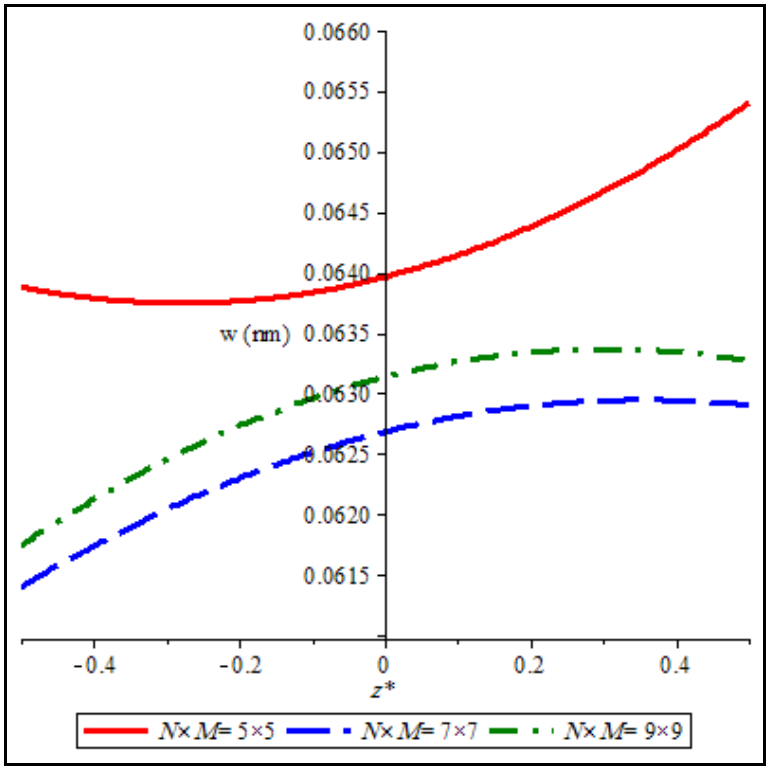

(b) CFCF boundary condition

Figure 3. Effect of the grid points distribution $N \times M$ on the deflection w (nm) along the dimensionless thickness direction z^*.
($L_x = L_y = 1.5\text{nm}$; $h = 0.34\text{nm}$; $E = 1.06\text{TPa}$; $\nu = 0.29$; $q_z = 10\text{GPa}$)

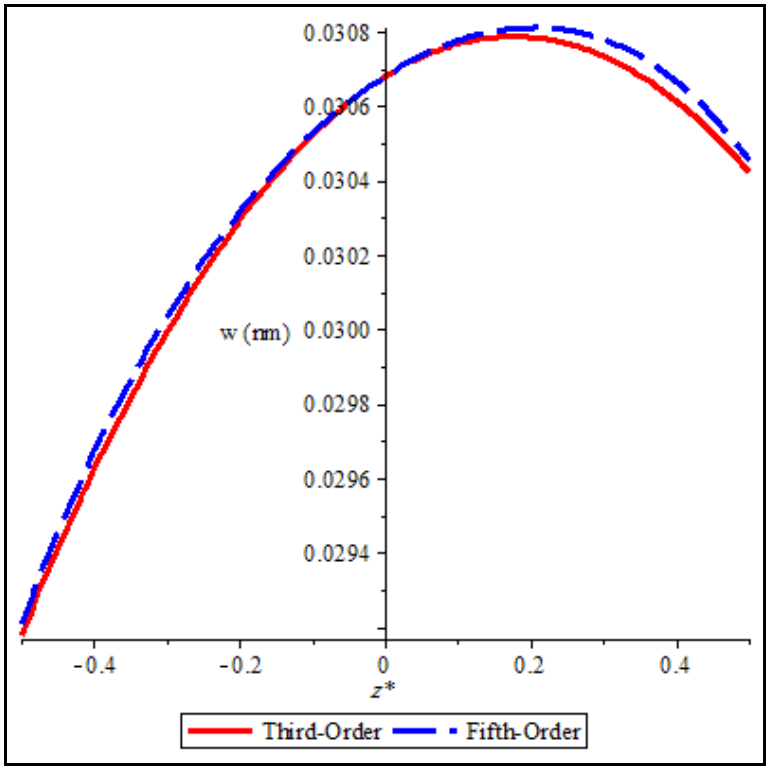

(a) CCCC boundary condition

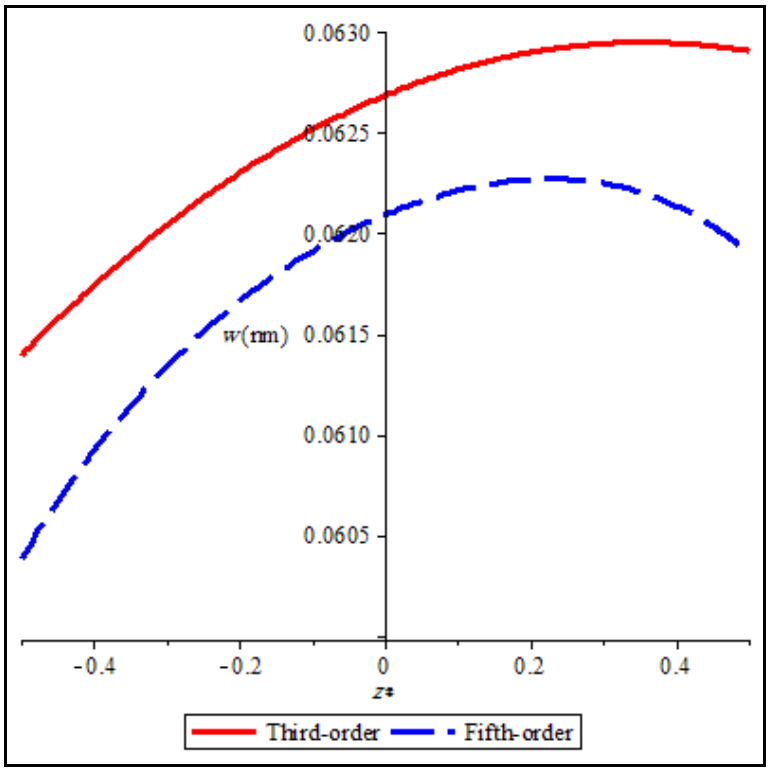

(b) CFCF boundary condition

Figure 4. Comparative evaluation of the deflection w (nm) along the dimensionless thickness direction z^* for a third-order or a fifth-order expansion.
($L_x = L_y = 3\text{nm};\ h = 1\text{nm}; E_m = 201\text{GPa}; E_c = 602\text{GPa};\ \nu = 0.25;\ q_z = 1\text{GPa};\ e_0 a = 0$)

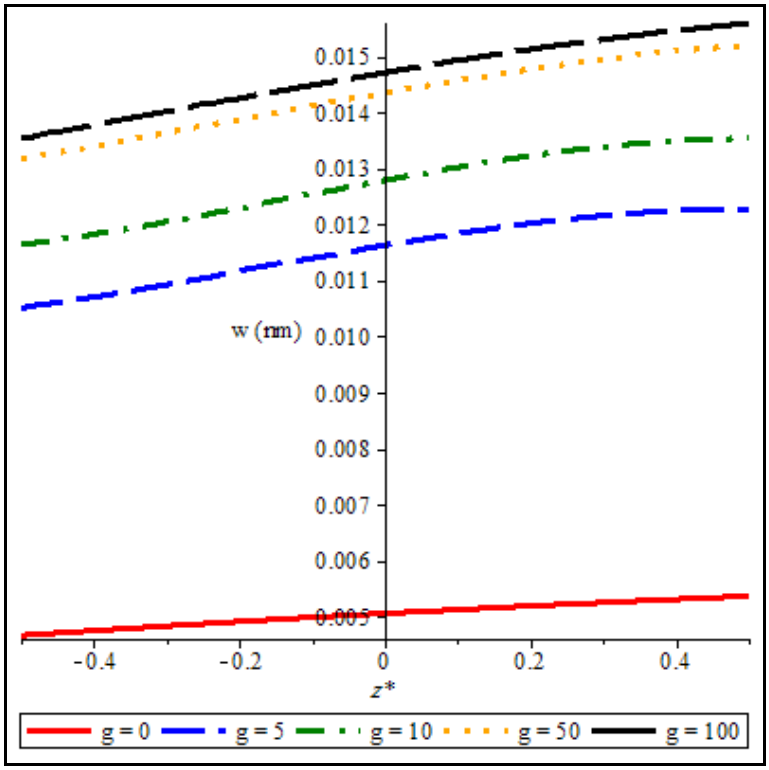

(a) CCCC boundary condition

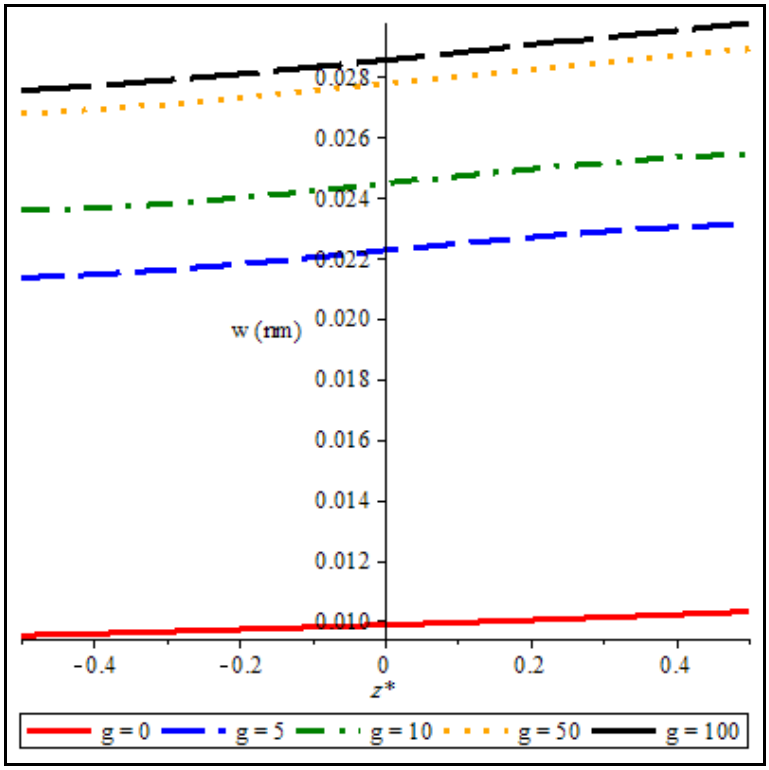

(b) FCFC boundary condition

Figure 5. Effect of the grading index g on the structural deflection.
$\left(h = 0.5\text{nm}; E_m = 201\text{GPa}; E_c = 602\text{GPa}; \nu = 0.25; e_0 a = 0; k_w = 1.13\text{GPa/nm}; k_p = 1.13\text{Pa×m}\right)$

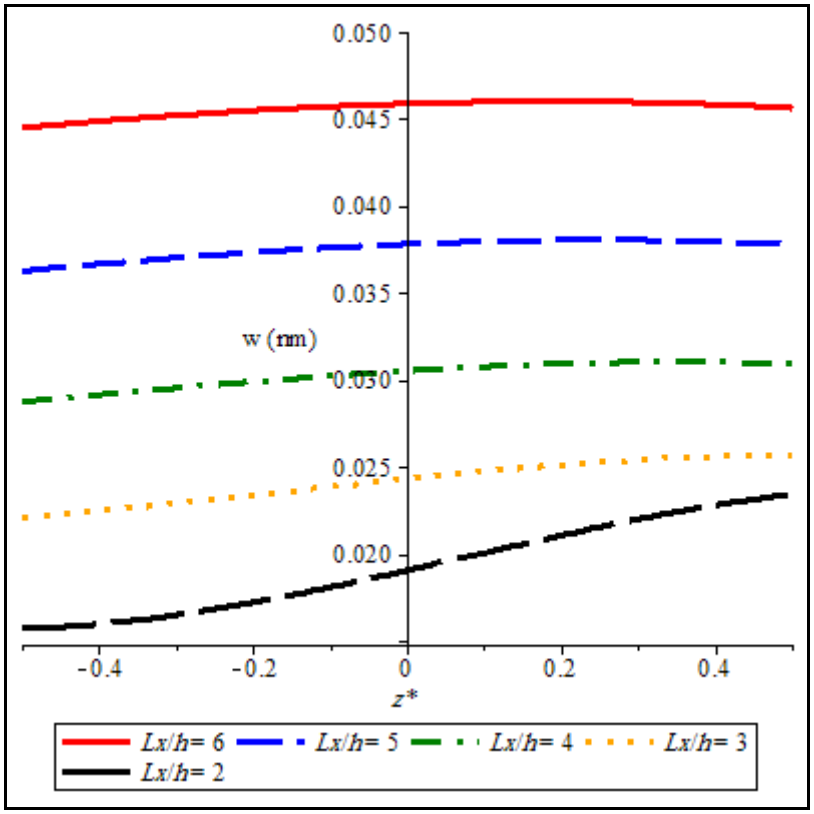

Figure 6. Effect of the dimensionless ratio L_x/h on the structural deflection $w(z)$. ($e_0a = 0; k_w = 1.13\text{GPa/nm}; k_p = 1.13\text{Pa}\times\text{m}$)

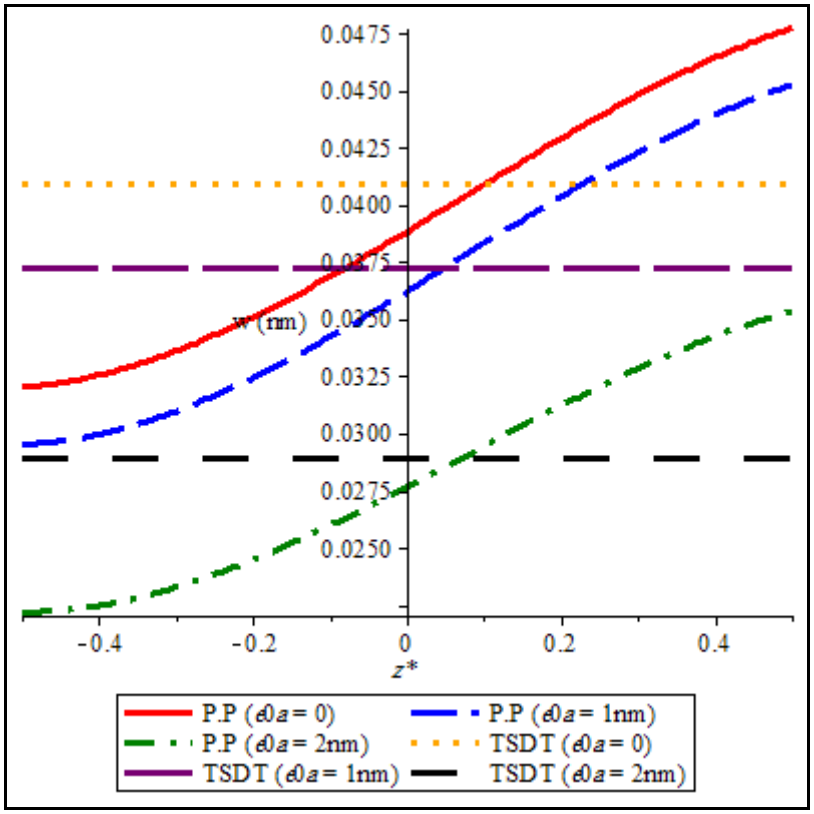

Figure 7. Effect of the nonlocal parameter $e_0 a$ on the results as given by the formulation proposed in the present paper and by a classical TSDT.
($L_x = L_y = 2\text{nm}; h = 1\text{nm}; E_m = 201\text{GPa}; E_c = 602\text{GPa};\quad g = 10;\ \nu = 0.25;\ q_z = 9\text{GPa}$;
$k_w = 1.13\text{GPa/nm}; k_p = 1.13\text{Pa}\times\text{m};$ Boundaries: CCCC)

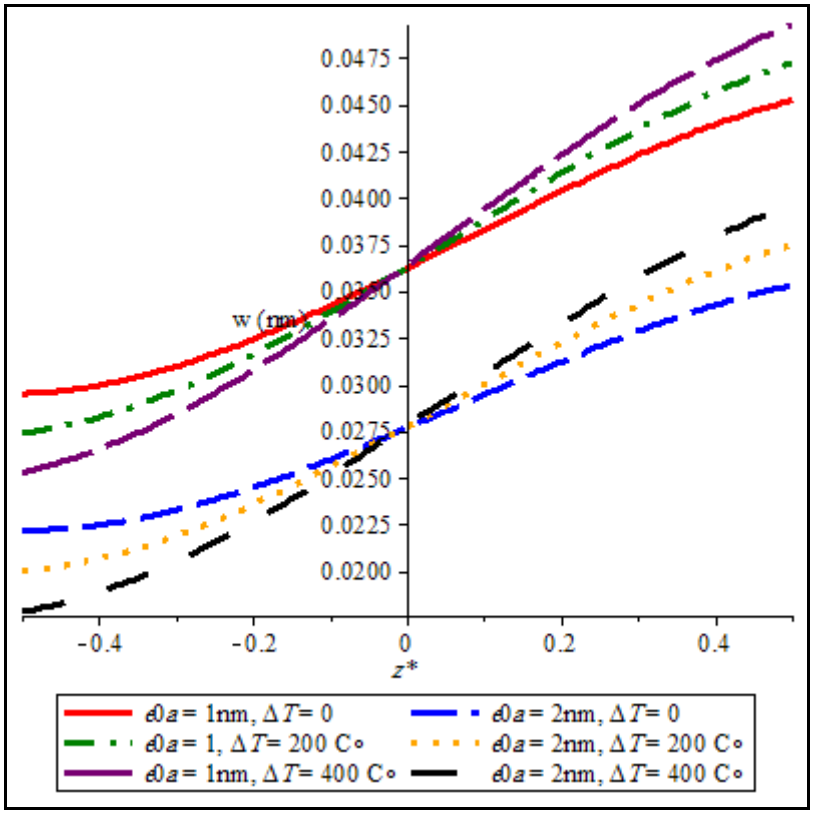

Figure 8. Thermo-elastic response for different values of $e_0 a$ and ΔT .

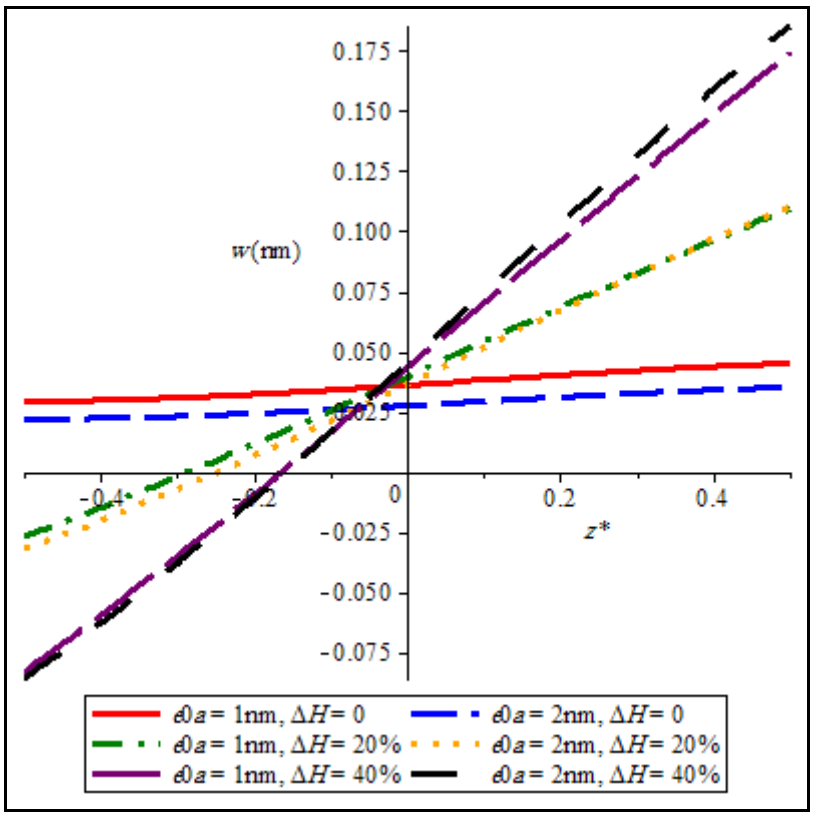

Figure 9. Effect of humidity on the results of $w(z)$ for different values of nonlocal parameter and ΔH .

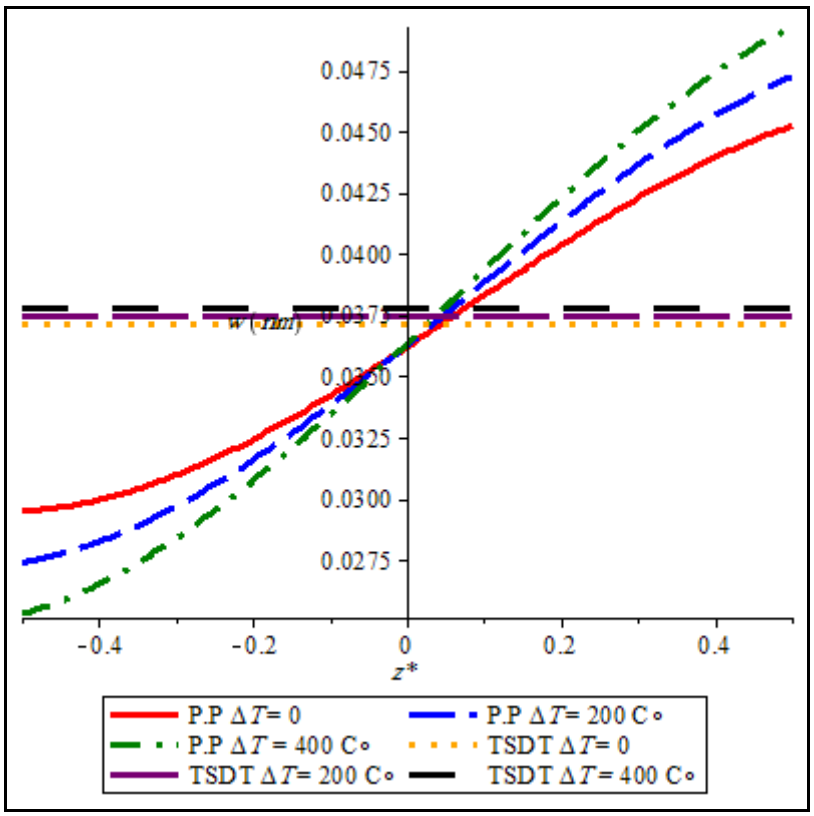

Figure 10. Comparative evaluation of the results, as given by the formulation proposed in the present paper and a TSDT, for different values of ΔT .

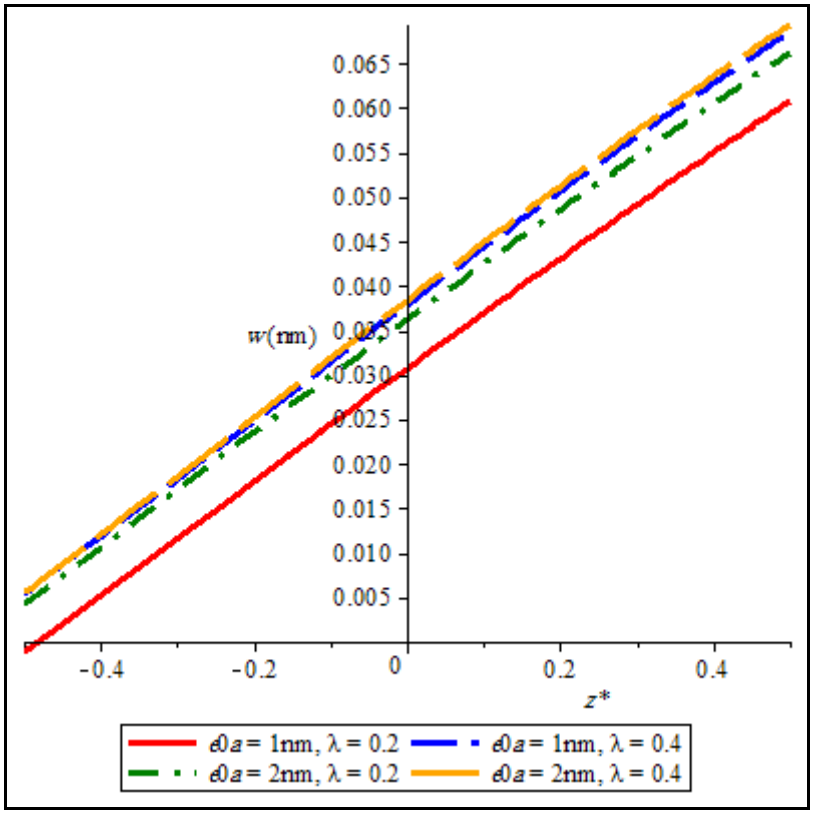

(a) Uneven porosity

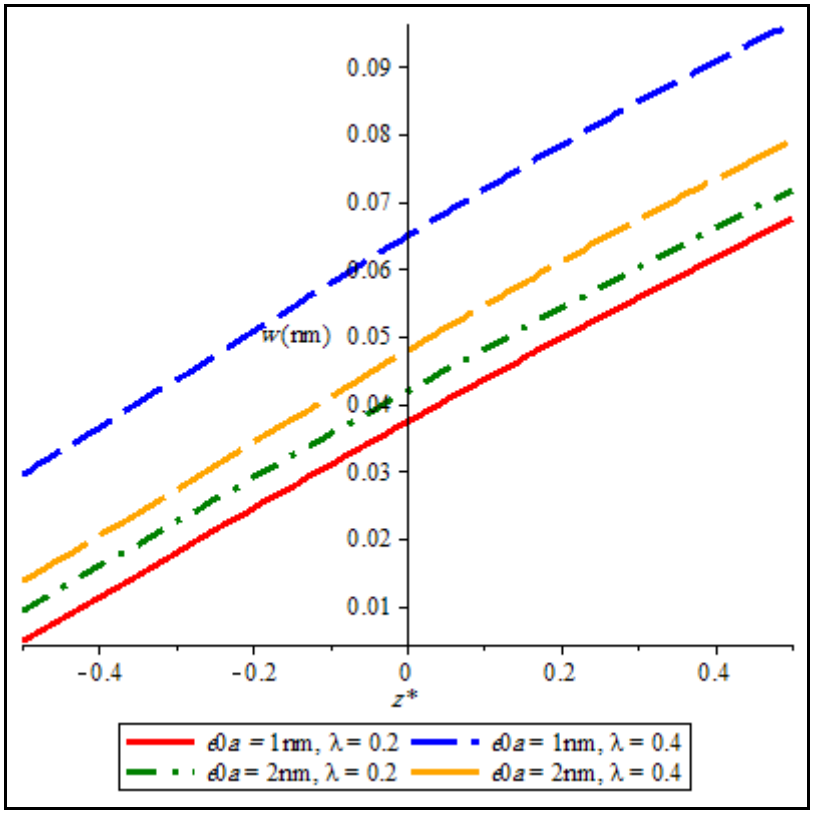

(b) Even porosity

Figure 11. Deflection vs. the dimensionless thickness for different values of the nonlocal parameter and porosity distributions.

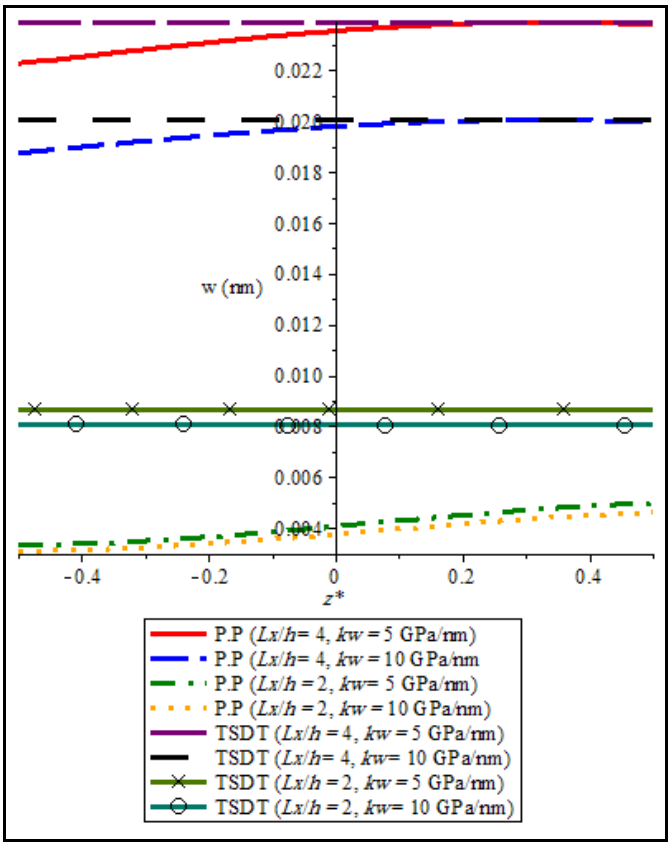

(a) Winkler foundation

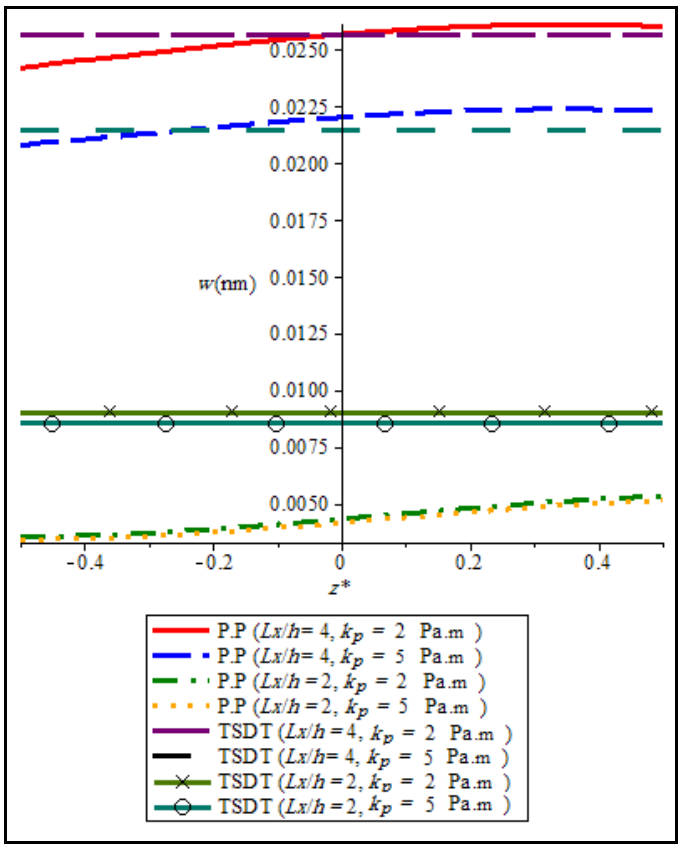

(b) Pasternak foundation

Figure 12. Effect of the elastic foundation parameters on the structural deflection. $e_0 a = 1\text{nm}$.

Table 1. Comparative evaluation of the kinematic response according to the present formulation, or according predictions from ABAQUS and TSDT, for different values of the thickness h and boundary conditions.

	$w(h/2)$ (m)			
	h (m)	ABAQUS	Present results	TSDT
CCCC	0.1	16.5	15.9	16.5
	0.2	2.79	2.68	2.79
	0.5	0.53	0.52	0.48
CFCF	0.1	270	262	250
	0.2	37.0	35.8	34.3
	0.5	3.78	3.68	3.52

Table 2. First validation for the new quasi three-dimensional elasticity results with those ones obtained through several plate theories from literature.

Dimensionless deflection (w^*)					
FSDT [54]	CPT [55]	S-FSDT [57]	FSDT [56]	Present results	q_z (psi)
0.048	0.048	0.048	0.048	0.048	0.5
0.064	0.064	0.064	0.064	0.063	1.0
0.083	0.083	0.076	0.083	0.081	2.0
0.090	0.089	0.078	0.088	0.088	2.5

0.096	0.095	0.085	0.095	0.095	3.0

Table 3. Second validation for the new quasi three-dimensional elasticity results with those ones obtained through several plate theories from literature.

w^*						
S-FSDT [57] e_0a		FSDT [55] e_0a		Present result e_0a		q_z (MPa)
0	0.8nm	0	0.8nm	0	0.8nm	
0.1035	0.0956	0.1037	0.0960	0.1035	0.0958	20
0.1377	0.1208	0.1382	0.1274	0.1380	0.1221	40
0.1544	0.1396	0.1609	0.1488	0.1550	0.1435	60

Table 4. Mechanical properties of the modeled FG porous nanosheet.

FG porous nanosheet ($\beta = 0.33$ $(wt.\ \%H_2O)^{-1}$) [58-61]	Porous metal; Stainless steel-grade 304 (SUS304) $E_m = 201\text{GPa}$, $\alpha_m = 12\cdot10^{-6}\,\text{K}^{-1}$, $\nu_m = 0.3262$
	Nano-oxide ceramic; Silicon carbide (SiC_4) $E_c = 602\text{GPa}$, $\alpha_c = 5\cdot10^{-6}\,\text{K}^{-1}$, $\nu_c = 0.1\,\nu_c$=0.1